

UNIVERSIDAD SAN FRANCISCO DE QUITO USFQ

Colegio de Ciencias e Ingeniería

**Methods for measuring the crystallinity
index using X-ray diffraction**

Ariana Elizabeth Soria Salgado

Física

Trabajo de titulación presentado como requisito
para la obtención del título en Física

Mayo 23, 2023

UNIVERSIDAD SAN FRANCISCO DE QUITO USFQ

Colegio de Ciencias e Ingeniería

**HOJA DE CALIFICACIÓN DE TRABAJO DE FIN DE
CARRERA**

Methods for measuring the crystallinity
index using X-ray diffraction

Ariana Elizabeth Soria Salgado

Profesores: Dario Niebieskikwiat, PhD
Christian Luciani, Encargado Laboratorios USFQ

Mayo 23, 2023

© Derechos de Autor

Por medio del presente documento certifico que he leído todas las Políticas y Manuales de la Universidad San Francisco de Quito USFQ, incluyendo la Política de Propiedad Intelectual USFQ, y estoy de acuerdo con su contenido, por lo que los derechos de propiedad intelectual del presente trabajo quedan sujetos a lo dispuesto en esas Políticas.

Asimismo, autorizo a la USFQ para que realice la digitalización y publicación de este trabajo en el repositorio virtual, de conformidad a lo dispuesto en la Ley Orgánica de Educación Superior del Ecuador.

Nombres y apellidos: Ariana Elizabeth Soria Salgado

Código: 00332599

Cédula de Identidad: 1718927203

Lugar y fecha: Mayo 23, 2023

ACLARACIÓN PARA LA PUBLICACIÓN

Nota: El presente trabajo, en su totalidad o cualquiera de sus partes, no debe ser considerado como una publicación, incluso a pesar de estar disponible sin restricciones a través de un repositorio institucional. Esta declaración se alinea con las prácticas y recomendaciones presentadas por el Committee on Publication Ethics COPE descritas por Barbour et al. (2017) Discussion document on best practice for issues around theses publishing, disponible en <http://bit.ly/COPETheses>

UNPUBLISHED DOCUMENT

Note: The following capstone project is available through Universidad San Francisco de Quito USFQ institutional repository. Nonetheless, this project – in whole or in part – should not be considered a publication. This statement follows the recommendations presented by the Committee on Publication Ethics COPE described by Barbour et al. (2017) Discussion document on best practice for issues around theses publishing available on <http://bit.ly/COPETheses>

Agradecimientos

Agradezco a mi familia, profesores, amigos, amigas. Dedicado a todas las personas que han formado parte de mi vida, porque cada una de ellas ha contribuido a formar la versión que soy ahora. Agradezco a Darío por su tutela a lo largo de este trabajo y a Christian por su apoyo incondicional.

Resumen

En el presente trabajo se realiza una revisión de los métodos disponibles para el cálculo del índice de cristalinidad en celulosa. Este cálculo es muy importante ya que existen grandes industrias que estudian a fondo las propiedades de la celulosa, las cuales dependen del porcentaje de celulosa cristalina presente en la muestra. Además, se realiza un estudio para mezclas de material cristalino (silicio) y amorfo (óxido de silicio) con la finalidad de entender mejor cómo se comporta el índice de cristalinidad. Finalmente se busca cómo aplicar este aprendizaje a muestras de celulosa.

Palabras clave: *celulosa, rayos-x, patrón de difracción, índice de cristalinidad, métodos disponibles, material amorfo, material cristalino.*

Abstract

In the present work a review of the methods available for the calculation of the crystallinity index in cellulose is carried out. This calculation is very important since there are large industries that study in depth the properties of cellulose, which depend on the percentage of crystalline cellulose present in the sample. In addition, a study is carried out for mixtures of crystalline (silicon) and amorphous (silicon oxide) material in order to better understand how the crystallinity index behaves. Finally, how to apply this learning to cellulose samples is discussed.

Keywords: *cellulose, samples, crystalline material, amorphous material, x-ray, crystallinity index, methods, silicon, silicon oxide.*

Contents

1	Introduction	12
2	Methods	15
2.1	State of the Art	15
2.1.1	Amorphous materials	16
2.2	Sample Preparation	18
2.3	Experimental Set-up (Powder XRD)	20
3	Results	24
3.1	Methods for calculating CI	25
3.2	Experimental Results	30
3.2.1	Crystalline Silicon Powder	30

3.2.2 Amorphous Material: Glass	33
3.2.3 Combined Samples	37
3.2.4 Cellulose	50
4 Conclusions	55
Bibliografía	57

List of Tables

2.1	Samples Mixtures	20
2.2	Variable time/step configuration	22
3.1	Experimental Results for areas and percentage of crystalline mass. .	41
3.2	Results for CI's	50
3.3	Crystallinity indices for cellulose samples	54

List of Figures

2.1	Sample preparation instruments.	19
2.2	Bruker D8 ADVANCE	21
2.3	Sample preparation instruments.	22
2.4	Illustration of the subscans	23
3.1	Illustration of the Segal Peak Height method [1].	25
3.2	Illustration of the amorphous subtraction method [2].	28
3.3	X-ray powder pattern crystalline Silicon	31
3.4	Raw data for defining the baseline	31
3.5	Baseline	32
3.6	Area 100% Crystalline Silicon	33

3.7 X-ray powder pattern amorphous material: Silicon Oxide	34
3.8 Fitting for the amorphous material: Silicon Oxide	35
3.9 Area for the pure amorphous material	36
3.10 Area for the 10% Crystalline Silicon sample	38
3.11 Area of the amorphous contribution for the 10% Crystalline Silicon sample	39
3.12 Area for the 80% Crystalline Silicon sample	40
3.13 Mass Factor vs Areas Contribution	42
3.14 Rational fitting function	44
3.15 Atomic scattering factors of the elements Au, Ag, Cu, and Al as a function of $\sin(\theta)/\lambda$ [3].	47
3.16 Pesudo-Segal for 10% Crystalline Silicon Sample	49
3.17 XRD data for cellulose FA2	51
3.18 Amorphou fit for cellulose FA2	52
3.19 FA1 Amorphous Contribution.	53
3.20 JC-CA Amorphous Contribution.	53

Chapter 1

Introduction

Cellulose is one of the fundamental components of materials of vegetable origin, it is the most abundant organic bio-molecule. It is present in plants, wood, and natural fibers. For this reason, studies focused on cellulose are very abundant. For example, the wood and paper industry is greatly interested in cellulose products.

Cellulose can be found in biomass but also can be produced by some bacteria and sea animals [2], [4]. Nowadays, cellulose materials are tested to show if they can produce renewable energy or be used to make nanomaterials [5], [6]. Moreover, cellulose is a main polysaccharide used in applications ranging from drug delivery to packaging [7].

Since cellulose is a renewable and friendly material for the environment, chemicals and fuels derived from it are being highly studied. In all of these studies, an understanding of the molecular structure of cellulose is very important, because

physicochemical and mechanical properties depend on cellulose structures [8]. The crystallinity of cellulose affects mechanical properties, such as strength and stiffness. For instance, the strength of a bio-composite material can be increased by including highly crystalline cellulose.

To study cellulosic materials, the use of X-ray diffraction is still prominent. This technique helps us determine the degree of crystallinity of these materials [9], [10], [11]. However, there exist other methods to determine crystallinity in cellulose samples such as Raman spectroscopy, infrared spectroscopy, differential scanning calorimetry, sum frequency generation vibration spectroscopy, and solid-state nuclear magnetic resonance, among others.

X-ray diffraction cannot recover the cellulose crystallinity directly of a sample. Instead, it recovers the mass fraction of crystalline cellulose among the entire sample [8]. It is important to mention that the crystallinity level of a cellulose sample may include crystalline contributions from other crystalline materials besides cellulose. Many XRD crystallinity studies, do not obtain an absolute value for cellulose crystallinity but rather the relative crystallinity value. Absolute crystallinity is calculated using isotropic samples, where the area under the intensity curve is calculated for the crystalline contribution relative to the combined areas of crystalline and amorphous contributions.

Cellulosic materials, most of the time, have crystalline and amorphous domains in varying portions. The portions depend on the source and history [12]. Amorphous materials are non-crystalline structures that lack long-range order and periodicity [13]. These materials have an internal structure that cannot be defined

by a finite unit cell, even though sometimes they present localized order on small length scales. Non-crystalline materials exhibit strong Bragg diffraction. Their diffraction patterns are characterized by diffuse peaks and low intensities.

Amorphous materials are gaining importance in the industry because of their interesting physical properties. Quantification of amorphous materials is very important in the research fields of planetary sciences [14], [15], [16]. Also, the assessment of cellulose crystallinity is essential for optimizing the yield of cellulose products. The physical properties of cellulose and chemical behavior depend strongly on the arrangement of the cellulose molecules [7].

Also, to study non-crystalline materials the use of X-ray diffraction (XRD) is primarily used because of its robustness and availability [17], [18]. Some of the most famous methods for crystallinity analysis in XRD are the Segal peak height method, peak fitting, amorphous standards, and two-dimensional Rietveld refinement [19].

There are several methods to perform crystallinity calculations but no standard one exists. Recently, there has been an interesting discussion on comparisons between the XRD crystallinity analysis methods [8]. Most of the articles discuss differences between the Segal method, peak fitting, or amorphous subtraction method [19], [20].

The objective of this work is to review the different existing methods for the calculation of crystallinity indices for cellulose and, in addition, to calculate CI on test samples by modeling the amorphous material.

Chapter 2

Methods

2.1 State of the Art

In the early 1900s, the discovery of Bragg diffraction solved most problems involving crystalline structures. If we expose crystal-structures to X-rays and analyze the diffraction angles at which the peaks appear and the wavelength of the X-rays, the full structure of the crystal can be obtained [21].

This important method of studying crystal structures is known as “X-ray Crystallography”; it has even allowed us to know the structure of proteins [22].

Bragg’s law is based upon the translational symmetry of crystals, i.e., the description of the crystal structure is reduced to specifying the symmetry group and some lattice parameters. Therefore, lattice periodicity is crucial.

The discovery that cellulose has a crystalline structure was made in the 19th century by Carl Von Nageli [23]. Later, this result was completely verified using X-ray crystallography [24].

In order to be able to criticize with scientific grounds the most used method [9] to calculate crystallinity indices in cellulose, we need to show that this method does not give precise results. For this, it is necessary to know a priori the crystallinity index of the samples. The most widely used method is called the Segal height method. This method does not work well since it does not consider the area under the curve of a diffraction pattern but only the heights. For this reason, this method underestimates the amorphous contribution of cellulose and provides a great value for the crystallinity index. This will be explained in more detail in the next section.

The samples used will be combinations of glass as an amorphous material and silicon as a crystalline component. In this way, the crystallinity index of each sample will be known a priori and this real value can be compared with the theoretical results.

This chapter will explain in detail how the samples were prepared, as well as the experimental set-up with which the data was obtained.

2.1.1 Amorphous materials

For non-crystalline structures, the absence of sharp peaks and smooth structure factors is a consequence of no long-range order. Hence, it presents a far more

complex problem regarding the structural determination of amorphous materials.

The purpose of structural analysis is to determine the properties of a given material based on the structure it has from the atomistic point of view. The properties of the material are not determined by the absolute position of each atom but by the relative positions of the closest atoms (in the sense that they are closer enough to produce some physical interaction that is not negligible) [23].

Pair Distribution Function (PDF)

In standard crystallographic analysis, the Bragg peaks and diffuse scattering are treated separately and the structure is determined entirely based only on information obtained from the Bragg peaks. Additional information regarding deviations from the perfect lattice is obtained through the study of diffuse scattering. We know this approach fails when the structure is extensively disordered.

An alternative approach, which treats both Bragg and diffuse scattering on an equal basis, is the so-called total scattering technique [23], [25], where it is necessary to have data over a wide range of Q -values (data throughout the reciprocal space).

The Pair Distribution Function (PDF) method for structural analysis is based on the Debye scattering equation which was developed back in 1915 by Peter Debye. The Debye scattering equation is an alternative method to compute the diffraction pattern of a collection of solid grains, that do not rely on a requirement of crystalline periodicity [26]. Therefore, this method is useful for cases where the

samples are not idealized crystals such as amorphous materials or nanoparticles.

In 1927, Zernicke and Prins found out the Fourier transform the relationship between the real-space atomic pair density and the Q -space total scattering intensity [27].

In order to make a meaningful Fourier transform, we need total scattering data over a large range of Q (wavevector). But the atomic form factor and atomic displacement parameter can lead to a significant decrease at high Q . Experimentally, Q is measured in the reciprocal space and it is:

$$Q \equiv |Q| = \frac{4\pi \sin \theta}{\lambda} \quad (2.1)$$

where 2θ is the scattering angle and λ is the incident radiation wavelength. Even though PDF mathematical foundations were established a long time ago, it was not widely applied until recent decades as a consequence of technological innovation.

Using equation 2.1, we can transform the data we measured to information in the Q -space. Notice that this information will be normalized by the wavelength of the X-ray tube. Since Q is inversely proportional to λ , by using high energy (short wavelength), high Q -regions can now be accessed. This will make the quality of the Fourier transformation better [23], [28].

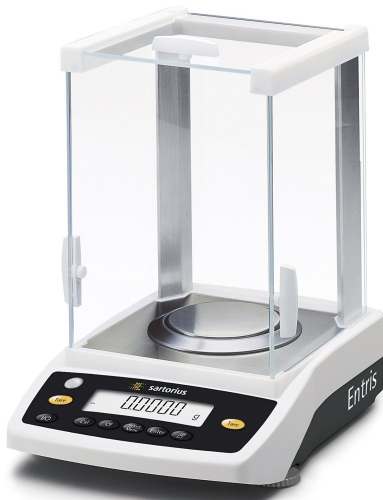
2.2 Sample Preparation

For this work, powder samples that were passed through the same experiment in a diffractometer were used. As a component of the crystalline material, mineral-

based 99.99% pure Silicon powder (100-200 mesh) from the ThermoFisher company was used. The safety data sheet for this compound is found in the appendices section. For the amorphous component, glass (Silicon oxide) between 120-230 mesh was used.

The samples used in this work are combinations between the crystalline material and the amorphous material, in such a way that the crystallinity index can be known a priori as the mass fraction of crystalline silicon.

A Sartorius Entris64-1S Analytical Balance was used to measure each component necessary to form each of the combinations at room temperature. For each combination, once the required amount of each compound had been carefully measured, a mortar and pestle were used to grind to a uniform sample for approximately one hour.



(a) Sartorius Analytical Balance.



(b) Agate mortar and pestle.

Figure 2.1: Sample preparation instruments.

Below is a table showing the sample amount of each pure component for 3 different mixtures:

Mass Factor [%]	Mass Crystalline Silicon [g]	Mass Silicon Oxide [g]
0	0.00	0.20
50	0.10	0.10
90	0.18	0.02

Table 2.1: Samples Mixtures

2.3 Experimental Set-up (Powder XRD)

X-ray diffraction was carried out at room temperature using the X-ray diffractometer D8 ADVANCE by Bruker. This equipment is designed to perform traditional X-ray powder diffraction (XRD), pair distribution function (PDF), small (SAXS), and wide (WAXS) angle X-ray scattering.



Figure 2.2: Bruker D8 ADVANCE

We performed standard powder diffraction experiments. The experiments were standardized. They were all carried out with the diffractometer using a cooper (Cu) K α radiation (wavelength 1.54 Å) at 50 kV and 20 mA, in θ -2 θ geometry.

All measurements were done using copper K α_1 energies ($\lambda = 1.5406 \text{ \AA}$), and K α_2 (1.54439 Å). The detector used was a Lynxeye XE (1D mode), and the rotation speed of the sample stage was 21 rotations per minute.

The PDS opening was set at 2.9493° and at a 280 mm goniometer radius. Samples used range from 0.1972-0.2000g. To perform the x-ray measurements, the samples were placed in a *Si* low background sample holder.

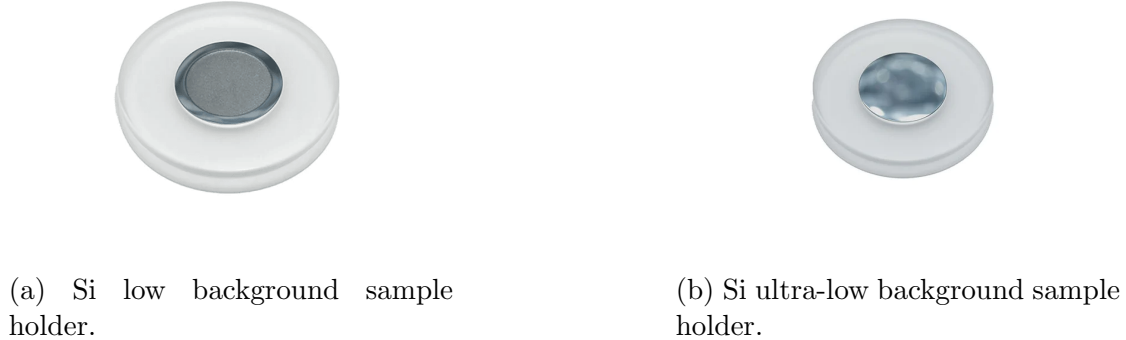


Figure 2.3: Sample preparation instruments.

The time taken to perform each measurement was 5 hours and 20 minutes approximately. Each of the experiment parameters was configured using Bruker's WIZARD. A more detailed account of the setup for each measurement is found in the appendices section.

Scans were obtained from 5 to 120 degrees 2θ using time-step variation depending on the 2θ angle, as follows:

From [°]	To [°]	Steps	Time/Step [s]
5	30	1221	1
30	60	2929	1.5
60	92	3125	2
92	120	2735	2.5

Table 2.2: Variable time/step configuration

Below is a graph of the time/step configuration used for each of the measure-

ments made:

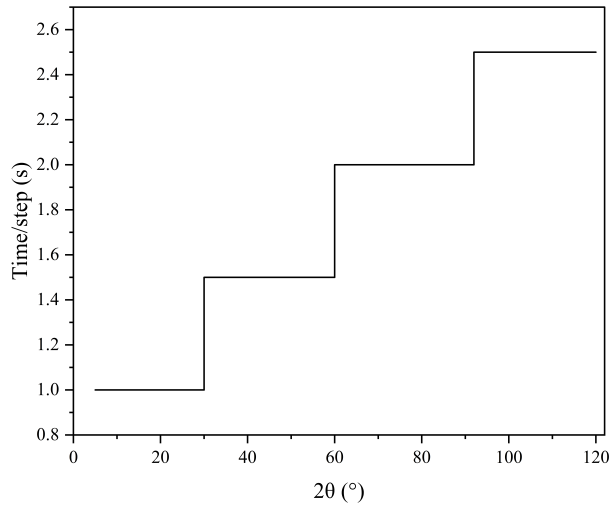


Figure 2.4: Illustration of the subscans

Chapter 3

Results

Several models for cellulose have been proposed since the discovery that cellulose has a crystalline part, but due to its complex structure is not fully understood yet. Cellulose samples have a significant portion that is less ordered; this portion is referred to as the amorphous part [1].

It is well-known that the method used to calculate the CI affects its value [29], [30]. The real CI values and the CI theoretical values are compared for each of the samples made. We calculated experimental CI values using 3 different approaches: Segal peak-height method [10], Eva software by Bruker, and our own amorphous fitting.

In this section, we will briefly discuss the available techniques using XRD to determine the crystallinity index (CI) for celluloses. Even though the scans where made from 5-120°, for the calculations we only used the information from 10-120°.

3.1 Methods for calculating CI

The most commonly used methods for calculating CI in cellulose samples are discussed below [9]:

Segal Method

The Segal method was proposed in 1959 by Segal, Creely, Martin, and Conrad [10]. They worked on an empirical method for determining the crystallinity of native cellulose using an X-ray diffractometer. They developed a simple equation from XRD:

$$CI = \frac{I_{200} - I_{am}}{I_{200}} \times 100 \quad (3.1)$$

where I_{200} is the height of the 200 peak and I_{am} is the height of the minimum between the 200 and the 101 peaks [1], [20].

Below is an image taken from Parker et. al. [1] to illustrate this method:

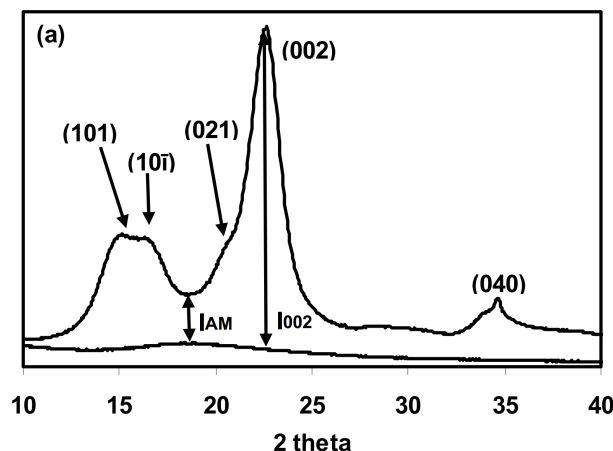


Figure 3.1: Illustration of the Segal Peak Height method [1].

This method has been suggested to be used when the purpose is to compare relative differences between samples. Authors have concluded that the method does not work well for estimating the amount of crystalline and amorphous material in cellulose samples for various reasons [1], [9].

Because the method focuses only on the highest peak (200) for the calculation of the CI, it excludes contributions from other crystalline peaks which puts too much emphasis on the contribution from one alignment of the cellulose crystal lattice. Furthermore, using intensity alone greatly underestimates the amount of amorphous cellulose in the sample.

Furthermore, peaks in the cellulose diffraction spectrum vary considerably in their width. Hence, a simple comparison of the heights cannot be expected to provide a reasonable estimation for CI [31].

Peak fitting methods

This method is the second most commonly used for determining CI; sometimes referred to as peak deconvolution. Peak fitting uses an amorphous standard or mathematical models for the amorphous contributions.

There are several ways to perform peak fitting. One of them is to model the amorphous component using a Gaussian peak. When using a Gaussian peak fitting without a linear background, we model the reflections (100), (110), (102), and (200) reflection peaks using Gaussian functions. A fifth Gaussian is used to model the amorphous contribution [9]. To obtain the CI value, we calculate the

area of the crystalline peaks as follows:

$$\text{CI} = \frac{A_{cr}}{A_{sample}} = \frac{\int_{2\theta_1}^{2\theta_2} I_{cr} d\theta}{\int_{2\theta_1}^{2\theta_2} I_{sample} d\theta} \quad (3.2)$$

where A_{sample} is the area under the sample intensity curve.

One of the main problems of the two methods briefly discussed above is the over-fitting of the amorphous components. If the fitting limits are too loose, the amorphous contributions will be unrealistic. In the case, they are too strict they will also affect in a negative way the CI value. For instance, if the lower limit for the width of the amorphous is too low, there exists a risk of fitting crystalline contribution with this peak and thus overfitting the amorphous contribution.

Another method uses a combination of a linear fit with a Gaussian peak. In this case, the amorphous model is more sophisticated. It is represented by a superposition of a linear fit and a wide Gaussian peak, with a peak maximum between 18° and 22° . The linear part of the fit is assumed to be part of the amorphous model [9]. Again, the CI value is calculated with the equation:

$$\text{CI} = \frac{A_{cr}}{A_{sample}} = \frac{\int_{2\theta_1}^{2\theta_2} I_{cr} d\theta}{\int_{2\theta_1}^{2\theta_2} I_{sample} d\theta} \quad (3.3)$$

Also, we cannot fail to mention the refinement of Rietveld refinement [32], which fits accurately the crystalline contribution and takes into account all crystalline diffraction peaks. In recent years, this method has been applied to the study of plant cellulose [33], [34].

Amorphous subtraction method

The amorphous subtraction method, also known as the Ruland-Vond Method, was developed in 1961 by Ruland and coworkers [35]. The method takes into account the scattering pattern of an amorphous sample or its corresponding model curve.

The crystallinity of the samples is calculated using the following equation:

$$CI = 1 - \frac{A_{am}}{A_{sample}} = 1 - \frac{\int_{2\theta_1}^{2\theta_2} I_{am} d\theta}{\int_{2\theta_1}^{2\theta_2} I_{sample} d\theta} \quad (3.4)$$

where A_{am} is the area under the amorphous curve and A_{sample} is the area under the curve intensity of the sample.

The amorphous subtraction method is based on the fact that the X-ray scattering intensities are quantitative values representing the volume fractions of the scattering components (crystalline and amorphous) [29].

This curve is fitted under the intensity curve of the studied sample and subtracted from the total intensity as shown in the following image taken from [29]:

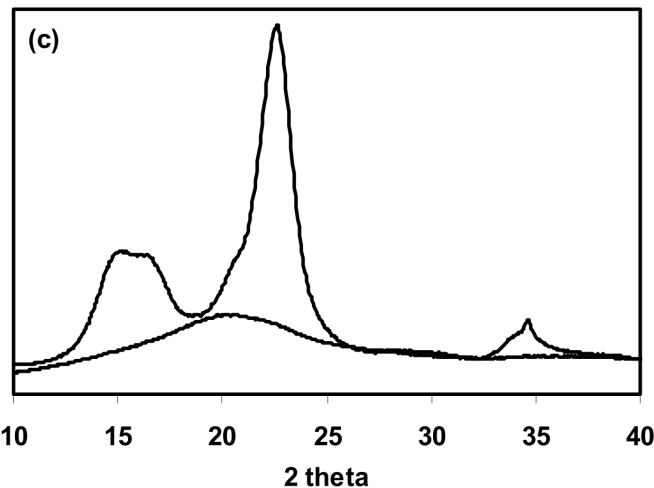


Figure 3.2: Illustration of the amorphous subtraction method [2].

It is important to mention that the amorphous curve is fitted to the data using a constant scaling factor so that the curve touches the experimental data at least one point but does not surpass it. Authors have stated that this method is sensitive to the exact shape of the amorphous standard. Because the amorphous model cannot surpass the sample intensity even if the model's shape is wrong in some part of the selected scattering angle range, we cannot quantify how well the chosen amorphous fits the data [9].

Amorphous fitting method

In this method, both the amorphous and the crystalline components are modeled. The most important step is to find a suitable model for the amorphous component. The amorphous fitting has a direct impact on the crystallinity values. It is necessary to find a chemically equivalent substance to the studied sample as the amorphous material. One of the most commonly used is ball-milled cellulose [29].

A linear superposition of the crystalline and amorphous models is used in the least squares fit. The equation for the crystallinity index (CI) is:

$$\text{CI} = 1 - \frac{A_{am}}{A_{sample}} = 1 - \frac{\int_{2\theta_1}^{2\theta_2} I_{am} d\theta}{\int_{2\theta_1}^{2\theta_2} I_{sample} d\theta} \quad (3.5)$$

The choice of the scattering angle region, the choice of the amorphous model, and the different corrections and background subtraction affect the crystallinity values obtained using this method. Furthermore, the method has been found to not be so good for determining whether a sample is fully crystalline. Also, it has been shown that amorphous subtraction is more sensitive to the exact shape of the amorphous standard than the amorphous fitting method [9].

3.2 Experimental Results

In this section, we discuss the experimental results obtained, the calculations made based on them, and their implications. All the results obtained have been processed using the Origin Pro 2023 software.

3.2.1 Crystalline Silicon Powder

Using the diffraction pattern obtained for the pure crystalline material (Silicon), we can analyze the introduction of a baseline for all measurements. This baseline takes into account the noise of the equipment used.

In order to obtain a more accurate and true baseline, we performed an experiment using only the ultra-low background sample holder which is made of monocrystalline silicon. The pattern obtained in the experiment will serve as a better guide to define the baseline of the equipment.

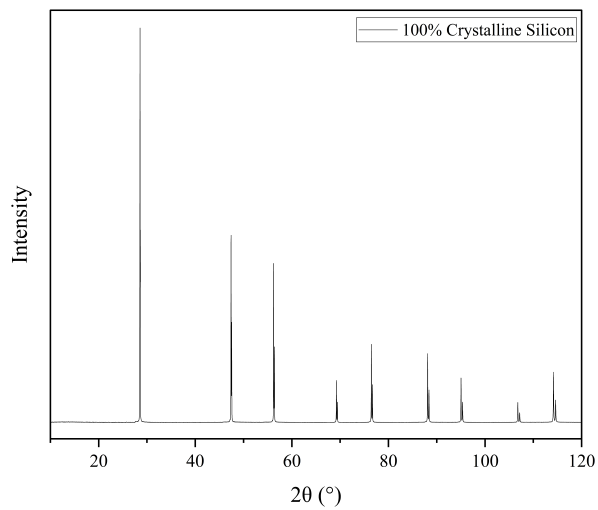


Figure 3.3: X-ray powder pattern crystalline Silicon

Below is a close-up of the background diffraction pattern for the ultra-low background Si sample holder and for the crystalline silicon powder:

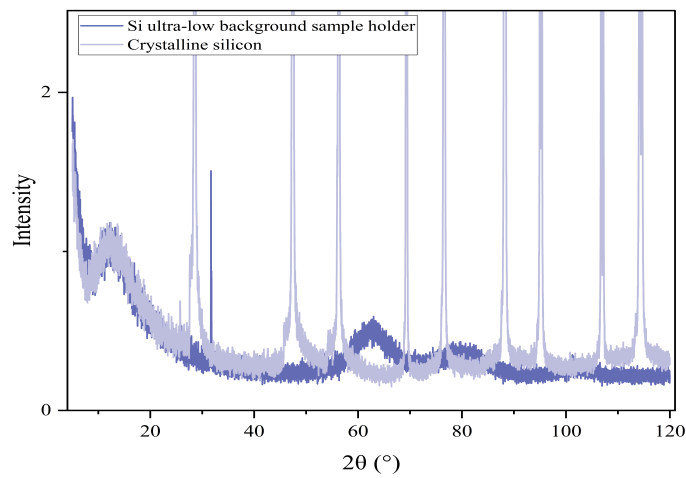


Figure 3.4: Raw data for defining the baseline

Looking at the two patterns of Figure 3.4, we decided to set a constant baseline starting at 50° . We define the baseline in such a way that we obtain the following function on the graph:

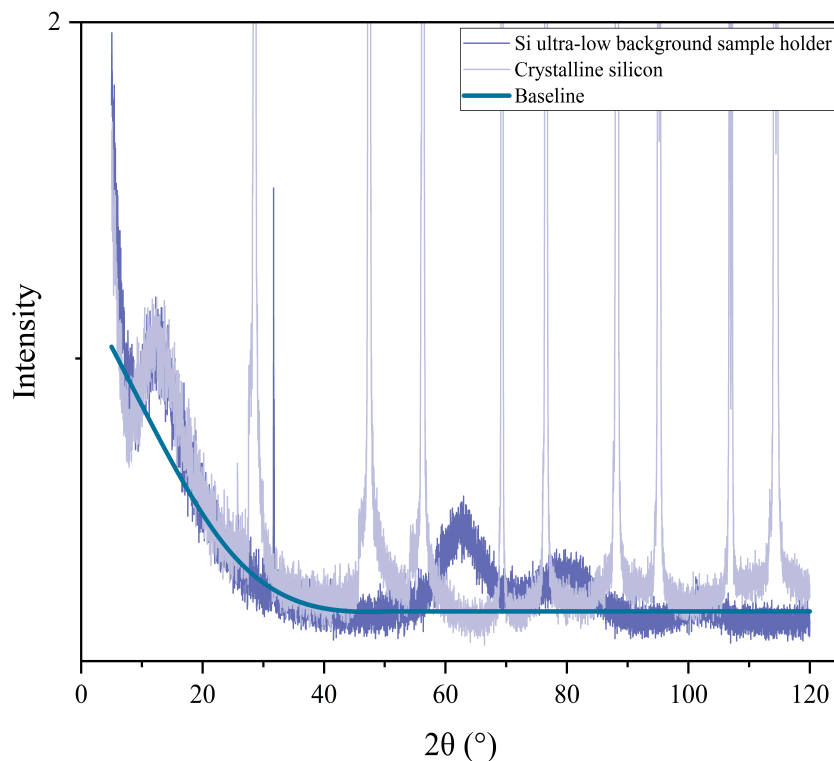


Figure 3.5: Baseline

Once we have defined the baseline, we must subtract said equipment contribution from all the measurements that have been carried out. In addition to allowing us to define the baseline based on XRD data, Origin Pro also lets us calculate the area under the curve from the data. In this way, we can know the area of the pure crystalline compound from $2\theta=10^\circ$ to $2\theta=120^\circ$, which by numerical integration gives:

$$P_c = 94.77 \quad (3.6)$$

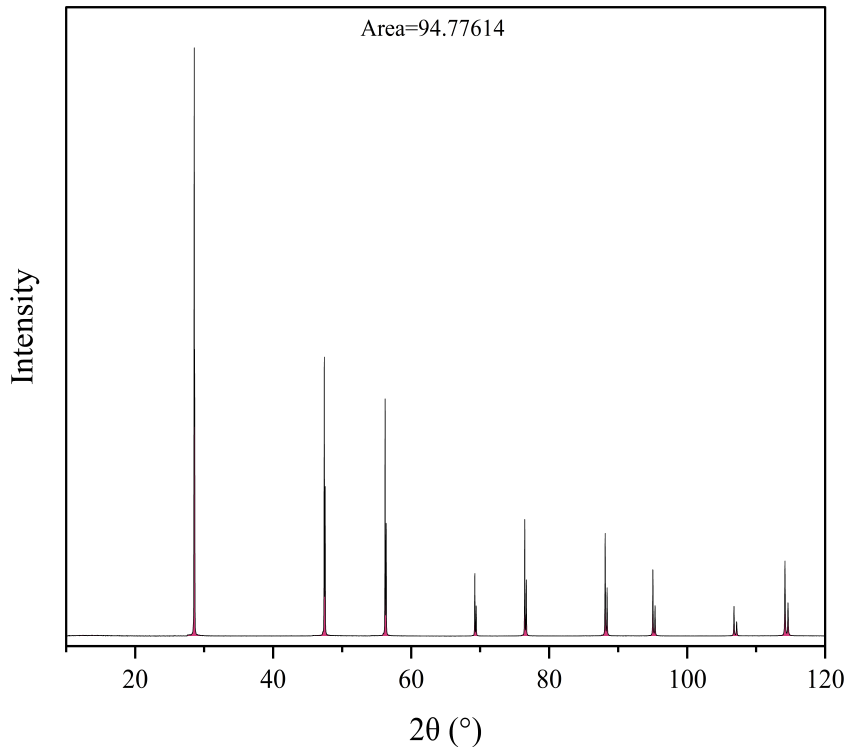


Figure 3.6: Area 100% Crystalline Silicon

3.2.2 Amorphous Material: Glass

For the amorphous compound of the mixtures that we will use for the study, there is 125-micron glass (silicon oxide). When observing the diffraction pattern of this material, we notice that it has the classical shape of amorphous materials. There are no marked peaks but a very broad humped peak. It is worth mentioning that a

63-micron glass sample was also studied but no significant difference was observed in the x-ray patterns obtained. For this reason, due to material availability issues, we use 125-micron silicon oxide.

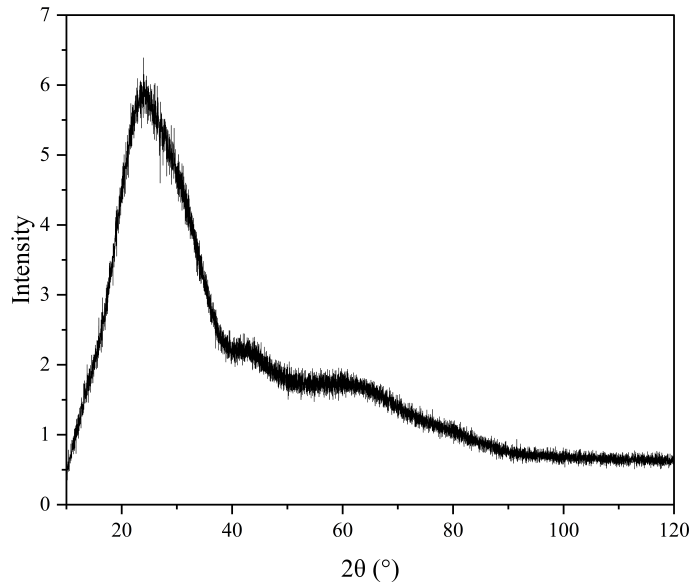


Figure 3.7: X-ray powder pattern amorphous material: Silicon Oxide

Using the x-ray diffraction pattern for the glass, we will look for a curve fit that allows us to model the contribution of the amorphous material to the diffraction patterns for each of the blends made. The function used to model the amorphous material, this function is a superposition of 3 asymmetric Gaussian functions plus a constant as defined below:

$$G(x) = G_1(x) + G_2(x) + G_3(x) + G_4(x)$$

where

$$G_1(x) = 0.6459$$

$$G_2(x) = \begin{cases} 5.08757 * \exp\left(-\frac{(x-24.12528)^2}{2.5.53823^2}\right) & \text{if } x < 24.12528 \\ 5.08757 * \exp\left(-\frac{(x-24.12528)^2}{2.9.16435^2}\right) & \text{if } x \geq 24.12528 \end{cases}$$

$$G_3(x) = \begin{cases} 1.03681 * \exp\left(-\frac{(x-44.32919)^2}{2.3.18844^2}\right) & \text{if } x < 44.32919 \\ 1.03681 * \exp\left(-\frac{(x-44.32919)^2}{2.13.77555^2}\right) & \text{if } x \geq 44.32919 \end{cases}$$

$$G_4(x) = \begin{cases} 0.63655 * \exp\left(-\frac{(x-63.89689)^2}{2.7.1627^2}\right) & \text{if } x < 63.89689 \\ 0.63655 * \exp\left(-\frac{(x-63.89689)^2}{2.14.40781^2}\right) & \text{if } x \geq 63.89689 \end{cases}$$

The diffraction pattern for glass and G functions are shown below:

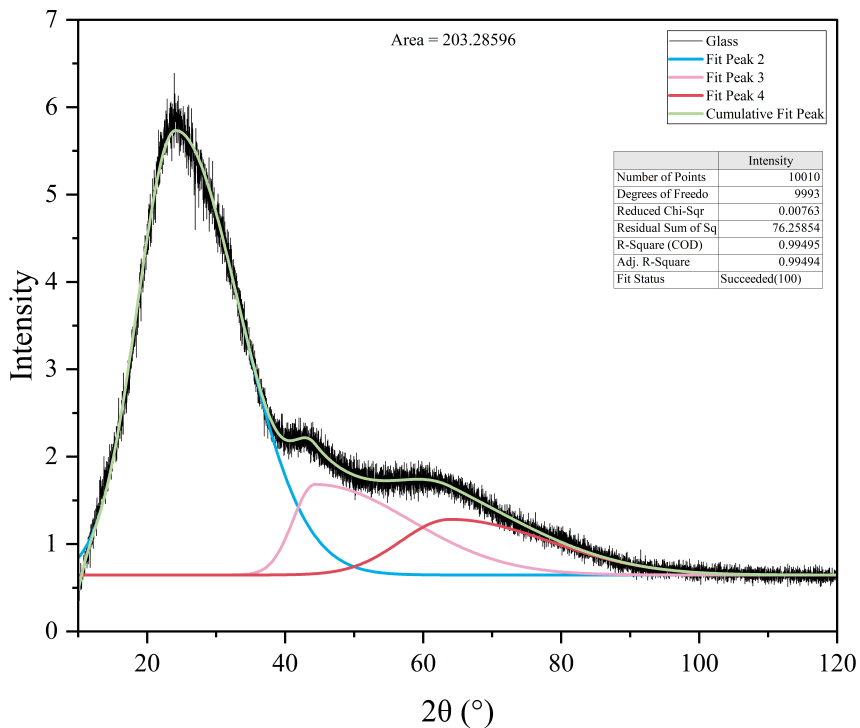


Figure 3.8: Fitting for the amorphous material: Silicon Oxide

With this model for the amorphous material, an adjusted R^2 coefficient of 0.99494 was obtained. These statistical values allow us to conclude that the proposed model fits the data well.

Once the function that models the x-ray pattern of silicon oxide has been obtained, we can numerically calculate the area under this curve in order to define the area of the pure amorphous material:

$$P_a = 203.28 \quad (3.7)$$

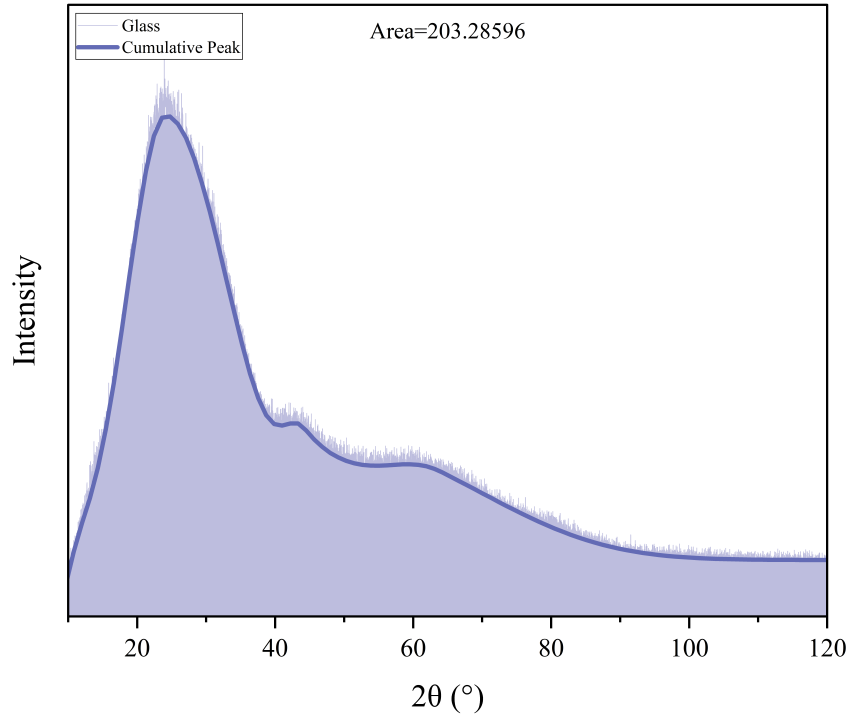


Figure 3.9: Area for the pure amorphous material

On the other hand, by scaling this model curve for amorphous material by a

numerical factor, we can estimate the amount of amorphous material present in a sample based on its x-ray diffraction pattern. This process will be explained in more detail.

3.2.3 Combined Samples

The process for calculating the area of a complete sample and the contribution to the area of its amorphous component is now discussed. The process is explained in detail for the case of the mixture of 10% Crystalline Silicon - 90% Silicon Oxide and 80% Crystalline Silicon - 20% Silicon Oxide.

10% Crystalline Silicon – 90% Silicon Oxide

Using the XRD data, we calculate the total area under the curve for this sample. We define for each sample the parameter of the total area as follows:

$$A_T = 187.88$$

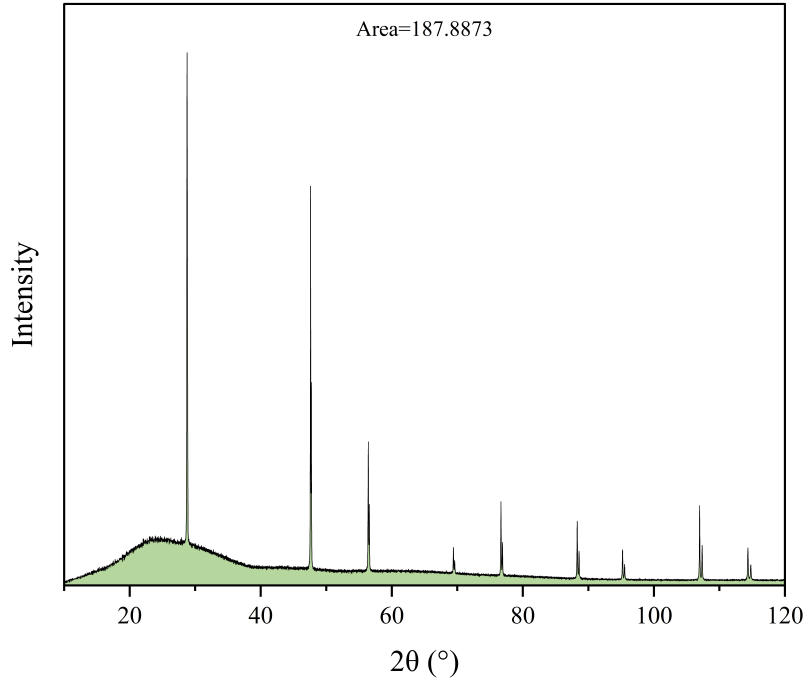


Figure 3.10: Area for the 10% Crystalline Silicon sample

Now, we need to calculate the area of the amorphous contribution. To do this, we plot our fitting curve model for pure glass in the XRD data plot for this sample. Then, we multiply the function $G(x)$ by a factor α so that the model curve fits the best to data. In this case:

$$\alpha = 0.90$$

$$\alpha = 0.90 \implies \tilde{G}(x) = 0.90G(x)$$

Graphically we have:

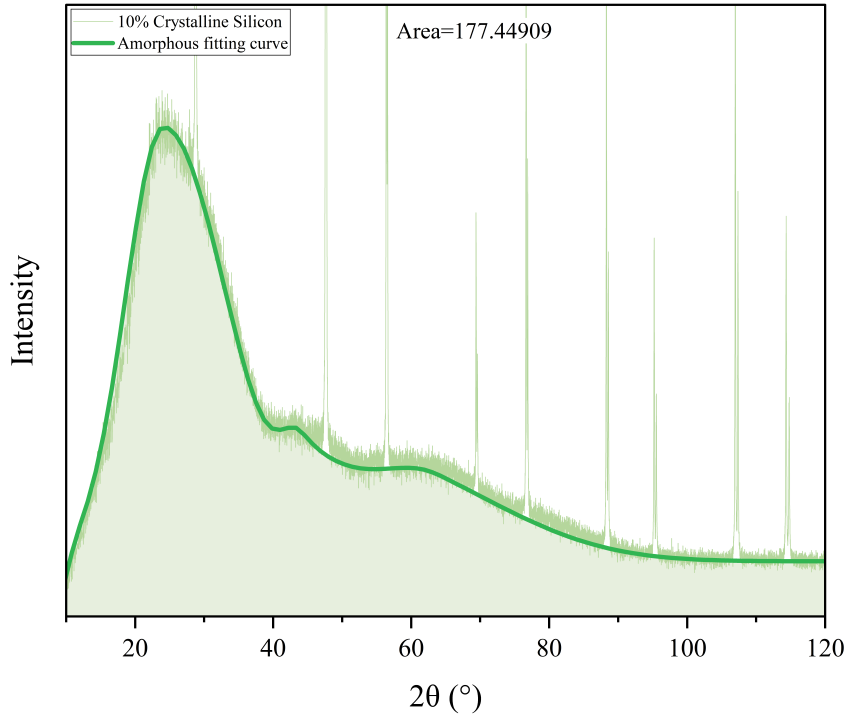


Figure 3.11: Area of the amorphous contribution for the 10% Crystalline Silicon sample

$$A_a = 177.44$$

Knowing the total area and the area of the amorphous contribution, we can determine the area of the crystalline part:

$$A_{cr} = 10.43$$

Hence, we obtain the ratio of areas for this sample (which is the percentage of crystalline material in the sample):

$$\begin{aligned} R &= \frac{A_{cr}}{A_T} \times 100 \\ R &= 5.55\% \end{aligned} \tag{3.8}$$

80% Crystalline Silicon – 20% Silicon Oxide

Using the diffraction pattern, we calculate the total area under the curve:

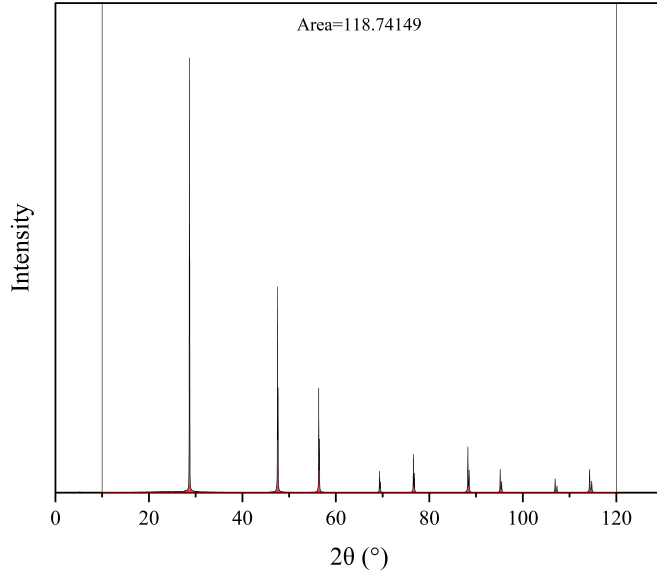


Figure 3.12: Area for the 80% Crystalline Silicon sample

$$A_T = 118.74$$

In this case, we multiply the function $G(x)$ by α so that the model curve fits the best to the data. In this case:

$$\alpha = 0.20 \implies \tilde{G}(x) = 0.20G(x)$$

We calculate the amorphous contribution to the total area by calculating numerically the integral of the function $\tilde{G}(x)$ from $2\theta=10^\circ$ to $\theta=120^\circ$. We obtain:

$$A_a = 41.68$$

Hence, the crystalline contribution to the area is:

$$A_{cr} = 77.05$$

Therefore, in this case:

$$R = \frac{A_{cr}}{A_T} \times 100 = 64.89\%$$

This process was carried out for each of the samples made. Finally, we obtained the following table:

Mass Factor [%]	Area		Crystalline Mass [%]
	Crystalline	Amorphous	
0	0	203.28596	0
1	1.53234	201.244	0.75568
2	1.9278	198.89457	0.95995
10	10.43821	177.44909	5.55557
20	17.3048	162.58078	9.61989
25	22.42028	138.8404	13.90313
30	32.6765	138.04989	19.13969
40	36.74056	125.79616	22.60447
50	48.39731	103.16031	31.93327
60	57.98769	82.12521	41.3864
70	67.84807	60.98303	52.66436
80	77.05337	41.68812	64.8917
85	81.84725	30.49151	72.85753
90	90.71659	20.32768	81.69408
100	94.77614	0	100

Table 3.1: Experimental Results for areas and percentage of crystalline mass.

Using the information in Table 3.1, we can plot the dependence of the amorphous and crystalline area contribution on the actual crystallinity index.

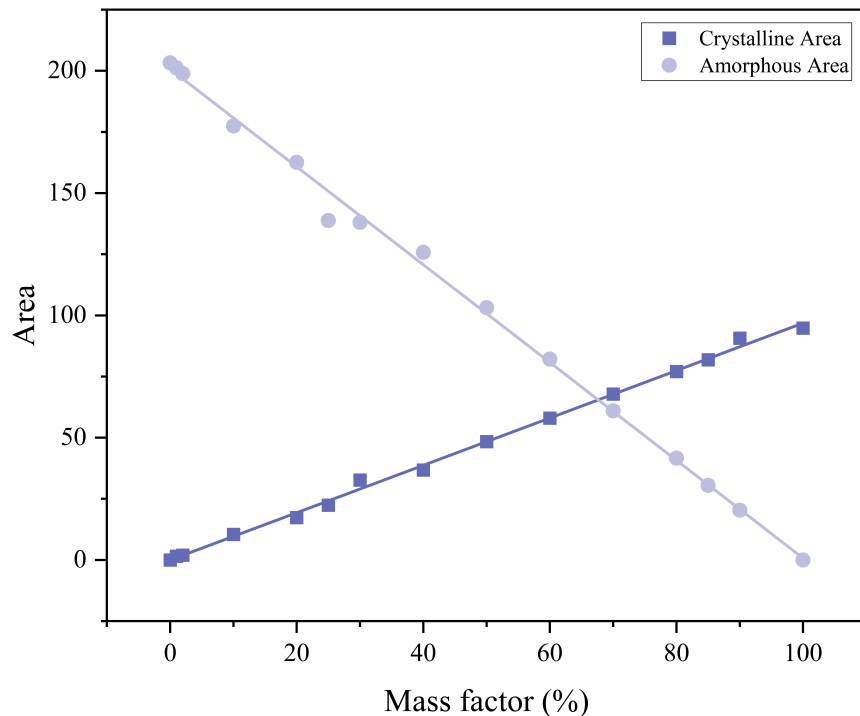


Figure 3.13: Mass Factor vs Areas Contribution

This graph allows us to observe that as the actual crystallinity index increases, the contribution to the total area of the amorphous part of the sample decreases linearly while the contribution of the crystalline part increases. Although this result may sound expected, it helps us to corroborate that the preparation of the samples and the operation of the equipment are adequate to carry out studies of crystallinity indices, and that the area under the two curves (crystalline and amorphous) is directly proportional to the respective mass fraction.

On the other hand, the curves in Figure 3.13 allows us to infer that the atomic

number of the contributions is not the same. It can be seen that the two contributions (crystalline part and amorphous part) have the same area when the actual crystallinity index is around 70% and not 50%.

Another way to look at this is to consider the ratio of the areas of the pure samples:

$$N \equiv \frac{P_a}{P_c} = \frac{203.28}{94.77} = 2.14 \quad (3.9)$$

That is, for the same amount of material, the amorphous part of a sample contributes more than twice the area of the crystalline part.

Now let us consider the analytical expressions for the contributions to the total area of a sample. The crystal contribution can be written as:

$$A_c = \frac{f}{100} P_c \quad (3.10)$$

where f is the percentage of the crystalline sample mass, also known as the mass factor (in our case also the real CI), and P_c is the total area of the pure crystalline material.

For the amorphous contribution:

$$A_a = \frac{100 - f}{100} P_a \quad (3.11)$$

where P_a is the total area of the pure amorphous material.

If we substitute equations 3.10 and 3.11 in 3.8, we get the following expression involving the the percentage of crystalline mass ($R \equiv C_{mass}$) and the mass factor (f):

$$R \equiv C_{\text{mass}} = \frac{100f}{f + 100N - fN} \quad (3.12)$$

where N is the ratio of areas:

$$N \equiv \frac{P_a}{P_c}$$

Using the information in Table 3.1, we can plot C_{mass} in dependence on the mass factor. By adjusting the form in equation 3.12 to these data we can experimentally obtain the ratio between the amorphous contribution and the crystalline contribution of the areas.

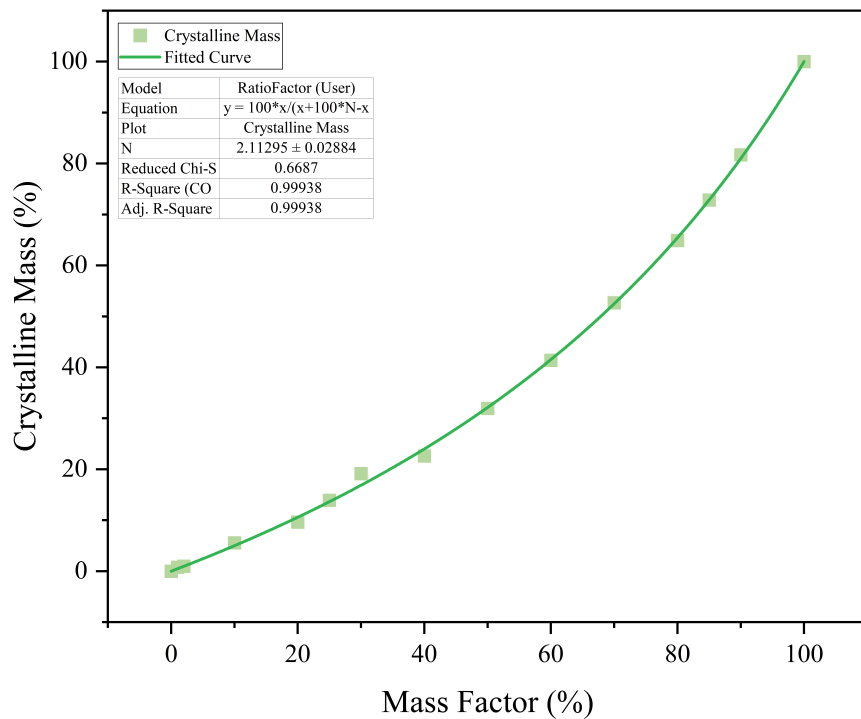


Figure 3.14: Rational fitting function

We get:

$$N = \frac{A_p}{C_p} = 2.11 \pm 0.03$$

Likewise, this value tells us that if we have the same amount of mass of crystalline and amorphous material, the amorphous area will contribute more than double that of the crystalline part.

A third way to calculate this ratio is to clear N from the equation 3.12:

$$N = \frac{100f - fC_{\text{mass}}}{C_{\text{mass}}(100 - f)} \quad (3.13)$$

Using the values of Table 3.1 for CI and CI_{exp} , we obtain a value for N for each sample. In this way, we get on average:

$$N = \frac{A_p}{C_p} = 2.04 \pm 0.25 \quad (3.14)$$

Now, we define the structure factor S [36]:

$$S_{\vec{G}} = \sum_j f_j \exp[-i2\pi(hx_j + ky_j + lz_j)] \quad (3.15)$$

where (hkl) are the Miller indices for a crystal. As can be seen in expression 3.15, the structure factor does not have to be real, since the intensity scattered is given by the product of $S_{\vec{G}}$ with its complex conjugate. The quantity f_j is a measure of the dispersing power of atom j . The structure factor S is important since the intensity of the X-rays is proportional to the square modulus of S .

The expression for the atomic form factor for X-rays is given by:

$$f_j = \int dV \eta_j(\rho) \exp[-i\vec{G} \cdot \vec{\rho}]$$

where $\eta_j(\rho)$ is the electronic density of the j -atom and $\vec{\rho} = \vec{r} - \vec{r}_j$. Since electronic density is seen as a property of atom j , the atomic shape factor is an atomic property.

If we consider a spherical symmetry of the electronic distribution, the vectors \vec{Q} and \vec{r} form an angle between them, and the molecule is made up of different atoms, the atomic form factor takes the following form:

$$f_j = 4\pi \sum_{j=1}^Z \int \eta_j(r) \frac{\sin(kr)}{kr} r^2 dr \quad (3.16)$$

This approximation is appropriate when the energy of the incident X-rays is high compared to the binding energy of the electrons [36].

In expression 3.16 there is a limit that occurs when the ratio tends to 1, this happens if the entire electron distribution lies at the origin. Hence, in this approximation the form factor is proportional to Z [37]. Structure factors often are approximate using computer programs by using atomic scattering factors (form factors) that are obtained by linear interpolation of experimental data. Linear interpolation is used to obtain the values of form factors from different atoms depending on resolution, expressed in units of $\frac{\sin(\theta)}{\lambda}$ [37], [38].

Here is an example of a graph with different atomic form factors for some elements of the periodic table:

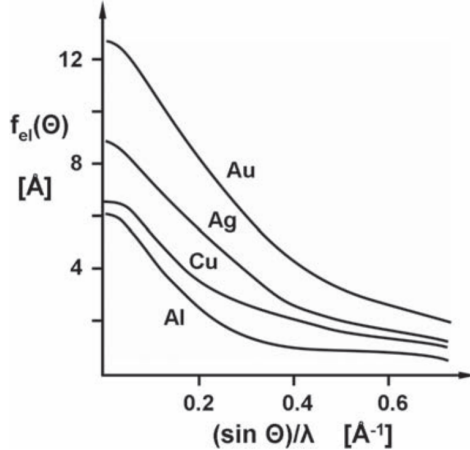


Figure 3.15: Atomic scattering factors of the elements Au, Ag, Cu, and Al as a function of $\sin(\theta)/\lambda$ [3].

Taking into account the elastic scattering approximation, much higher incident x-ray energy compared to the binding energy, and angles 2θ not greater than 100° , the form factor can be approximated to the atomic number Z [3], [39]. For the crystalline silicon we have:

$$f_{\text{Si}} = 14 \quad (3.17)$$

For silicon oxide:

$$f_{\text{SiO}_2} = 14 + 8 + 8 = 30 \quad (3.18)$$

Therefore:

$$N = \frac{f_{\text{SiO}_2}}{f_{\text{Si}}} \approx \frac{Z_{\text{Si}} + 2Z_{\text{O}}}{Z_{\text{Si}}} = \frac{30}{14} = 2.14285 \approx 2.14 \quad (3.19)$$

We note that this value, which is the ratio between the form factor of the amorphous material and the atomic form factor of the crystalline material, is very close to the values obtained for the area ratio present in expressions 3.9, 3.2.3,

3.14.

In conclusion, we have learned that for our mixtures it is not correct to consider that the amorphous area and the crystalline area contribute equally to the x-ray diffraction pattern.

Next, we will calculate the crystallinity index for our blends using different methods: Segal, Eva (by Bruker) and our amorphous fitting with area weight correction. To apply the weight correction for the areas contribution (which takes into account the atomic form factor), we calculate the inverse of the fitting equation of graph 3.14 (with N=2.11). We obtain the following expression for the CI based on the experimental crystalline mass obtained from equation:

$$CI = -\frac{100N}{C_{mass} - N \times C_{mass} - 100} C_{mass} \quad (3.20)$$

On the other hand, Bruker's Eva Software will be used to calculate the crystallinity index of the samples made. Given an x-ray diffraction pattern, this program makes a model for the amorphous part and using numerical integration gives us the crystallinity index based on areas calculation.

For the purpose of comparing the Segal method, we will perform a modified Segal for the silicon oxide samples - crystalline silicon. In this case we will take the height of the amorphous part of the samples as the maximum intensity of the amorphous part (I_a), for the crystalline part the maximum intensity of the main silicon peak will be used (I_{200}), and then we apply equation 3.1.

Below is an illustrative example for the mixture of 10% crystalline silicon:

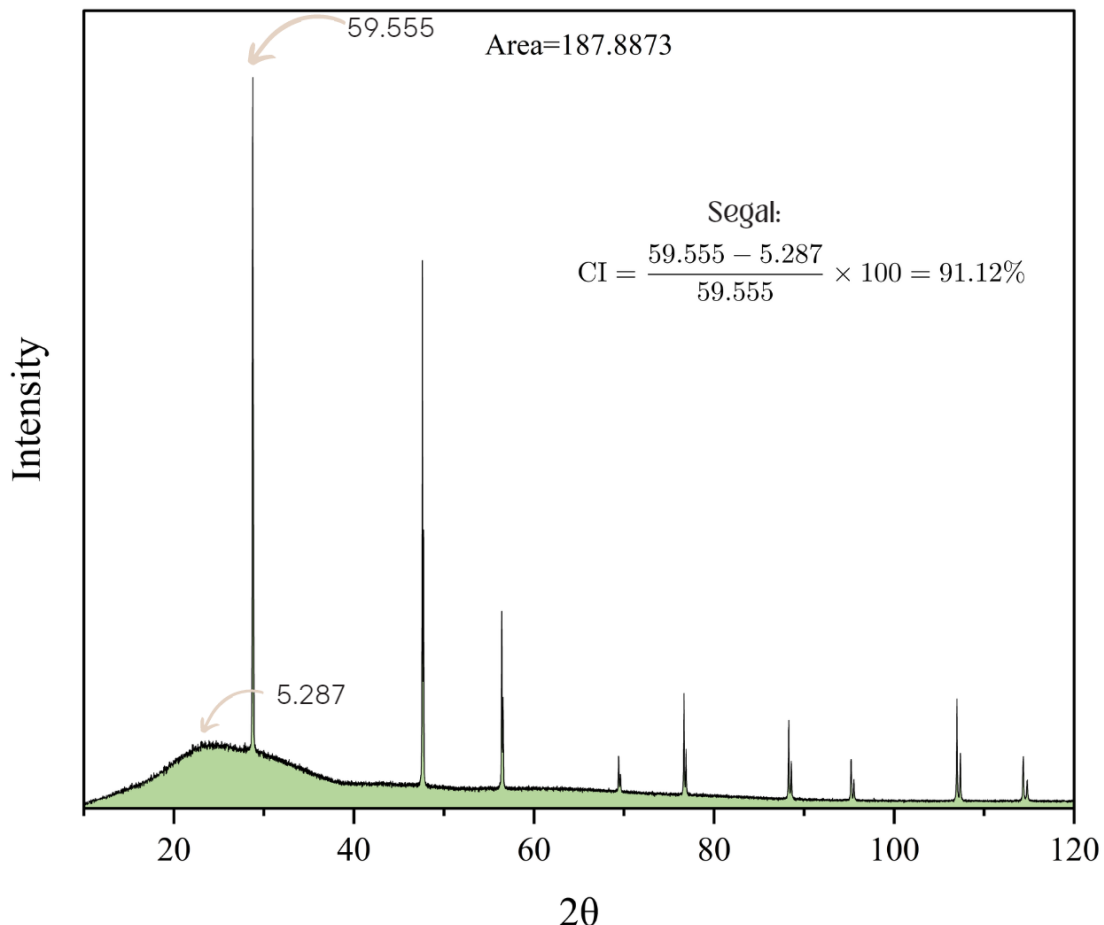


Figure 3.16: Pesudo-Segal for 10% Crystalline Silicon Sample

In this way we can calculate the crystallinity index for our mixtures made in the laboratory in three different ways and thus compare the values.

The results obtained indicate that the Segal method results in crystallinity indexes that are too high, taking into account the amount of crystalline mass present in each sample. This is because in this extreme case, the intensity of the main peak of silicon is much higher compared to the maximum intensity of silicon oxide. On the other hand, this confirms the idea that making a height comparison

is not enough to provide a real value of the crystallinity index. The results for crystallinity index using the form factor correction and EVA are quite similar.

Below is the table with results:

Real CI [%]	Segal [%]	EVA [%]	Crystalline Mass [%]	Form-Factor Correction [%]
0	0.00	6.00	0.00	0.00
1	23.45	6.30	0.47	1.58
2	72.96	8.80	0.88	2.00
10	91.12	22.50	5.80	11.04
20	97.28	43.70	10.21	18.34
25	97.05	41.10	13.29	25.41
30	97.53	50.00	17.13	33.31
40	96.71	37.60	22.26	38.13
50	97.32	47.30	30.59	49.75
60	98.10	53.40	36.73	59.84
70	99.64	83.60	52.31	70.13
80	99.72	88.90	63.28	79.59
85	99.83	91.20	72.14	84.99
90	99.91	93.00	81.02	90.40
100	100.00	92.40	100.00	100.00

Table 3.2: Results for CI's

3.2.4 Cellulose

Once we have learned more thoroughly how the crystallinity index behaves, knowing what percentage of crystalline mass exists in a given sample, we can try to

apply this knowledge to the object of interest: cellulose.

Following the process described for the mixtures of silicon oxide and crystalline silicon, the first step is to find a mathematical model for the amorphous component present in the cellulose samples. To do this, the most amorphous cellulose sample from those available (provided by Prof. Frank Alexis from the USFQ chemistry department) is chosen. Since cellulose is widely studied, it is well known that the three main peaks (of crystalline origin) are located between $2\theta_1=14-16^\circ$, $2\theta_2=22-24^\circ$ and $2\theta_3= 33-35^\circ$ [40], [41]. This is important since we will use asymmetric Gaussian functions as before, but none should be centered in the positions that correspond to the crystalline peaks of the cellulose.

Below is the x-ray diffraction pattern for the most amorphous sample of cellulose available, where the crystalline peaks almost cannot be seen:

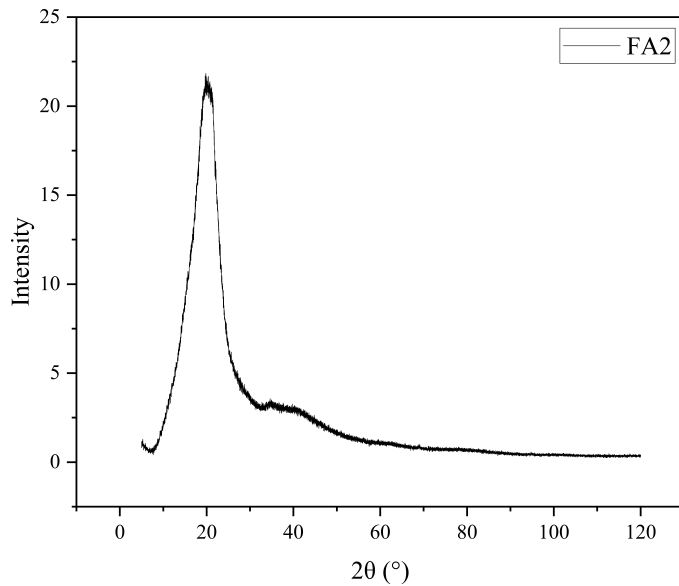


Figure 3.17: XRD data for cellulose FA2

Now the model curve for the amorphous part of the cellulose is presented, as well as the statistics obtained for the fitting.

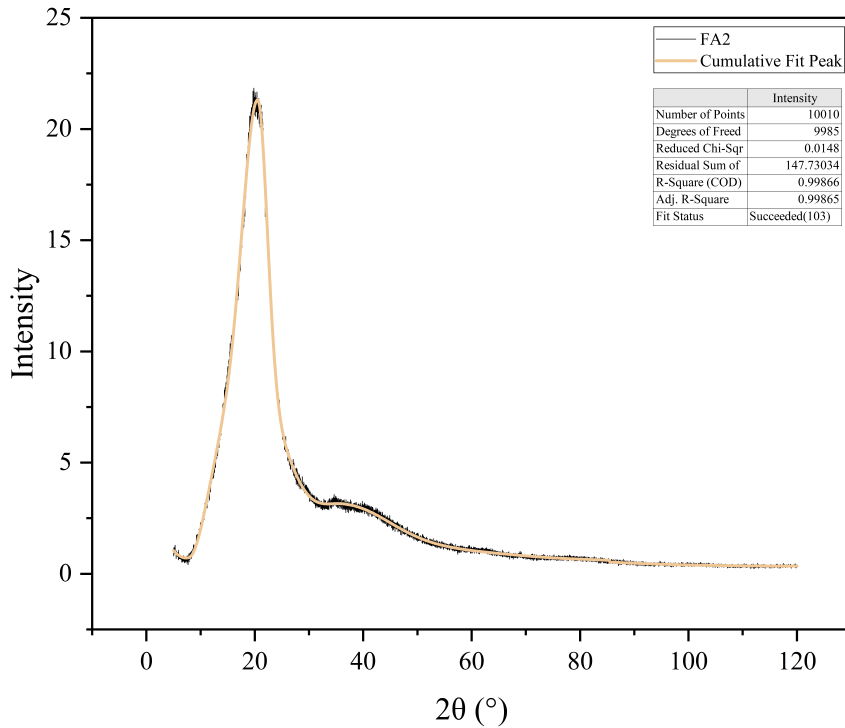


Figure 3.18: Amorphous fit for cellulose FA2

In addition to FA2, we will only study two more samples of cellulose FA1 and JC-CA. As before, we will now multiply the modeling function for the amorphous part of the cellulose $G(x)$ by a numerical factor α in such a way that the curve best fits the x-ray pattern for samples that contain a greater mixture between the crystalline and amorphous part.

We obtain the following scalings of the model function:

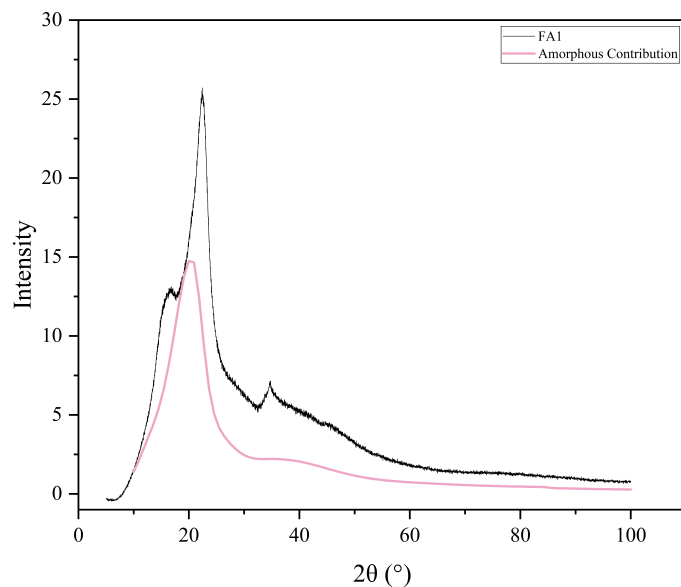


Figure 3.19: FA1 Amorphous Contribution.

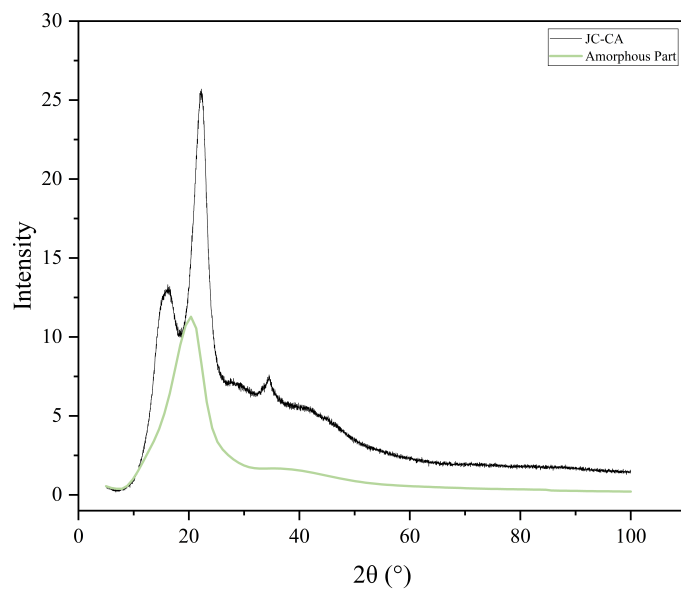


Figure 3.20: JC-CA Amorphous Contribution.

When trying to apply the same process used in the samples we manufacture, we found certain differences. Since the cellulose samples are made of the same material, there is only one form factor to take into account. However, when we try to apply a scaling of the modeling function to the amorphous part of the cellulose, we find that the amorphous part of the cellulose changes from sample to sample. This may be because the amorphous tries to order itself as the degree of crystallinity of the sample increases. That is, it is not possible to use a standard function for the amorphous part of cellulose samples. We have a different amorphous per cellulose sample.

In order to make comparisons of the Segal method and the Bruker software, we will calculate the crystallinity index of the cellulose samples, we can obtain the following results:

	EVA [%]	Segal [%]
FA2	7.50	19.21
FA1	12.50	41.16
JC-CA	20.80	59.21

Table 3.3: Crystallinity indices for cellulose samples

Chapter 4

Conclusions

Once this preliminary work is finished we can conclude (through our own experimentation) that the method used to calculate the crystallinity index of cellulose samples does affect the final result. We also note that the Segal method continues to be the most widely used, despite being the one that gives the most unreliable results, especially when applied to mixtures made of crystalline silicon and silicon oxide. This is because the intensity of the main silicon peak is much higher compared to the intensity resulting from the amorphous part of the mixture. For the cellulose samples we reached similar conclusions as other authors, the average sample crystallinity values for the Segal method are higher than for the other methods [9].

On the other hand, the contribution of the amorphous part of a mixture does not always have the same weight as its crystalline part. This has to do with the atomic number of a molecule which under certain assumptions is directly propor-

tional to the atomic form factor.

Furthermore, a very similar study can be performed with fabricated test samples with amorphous silicon instead of silicon oxide. In this case, we would expect the areas to contribute similarly by weight since the two compounds would have the same atomic number. This more homogeneous study at the molecular level could provide us with an even better understanding of the behavior of the crystallinity index so that it can be applied to cellulose.

With the learning obtained from experimenting with mixtures between known percentages of amorphous and crystalline material, it was possible to propose a model for the amorphous part of cellulose samples. However, we learned that a standard model for the amorphous part of cellulose cannot be applied.

Bibliography

- [1] Sunkyu Park, John O Baker, Michael E Himmel, Philip A Parilla, and David K Johnson. Cellulose crystallinity index: measurement techniques and their impact on interpreting cellulase performance. *Biotechnology for Biofuels*, 3(1), May 2010.
- [2] Dieter Klemm, Friederike Kramer, Sebastian Moritz, Tom Lindström, Mikael Ankerfors, Derek Gray, and Annie Dorris. Nanocelluloses: A new family of nature-based materials. *Angewandte Chemie International Edition*, 50(24):5438–5466, May 2011.
- [3] Barbara Marczevska and Krzysztof Marczevski. First glass electrode and its creators f. haber and z. klemensiewicz – on 100th anniversary. *Zeitschrift für Physikalische Chemie*, 224(05):795–799, May 2010.
- [4] Chisuzu Tokoh, Keiji Takabe, Minoru Fujita, and Hiroshi Saiki. Cellulose synthesized by acetobacter xylinum in the presence of acetyl glucomannan. *Cellulose*, 5(4):249–261, 1998.
- [5] Robert C. Armstrong, Catherine Wolfram, Krijn P. de Jong, Robert Gross, Nathan S. Lewis, Brenda Boardman, Arthur J. Ragauskas, Karen Ehrhardt-

- Martinez, George Crabtree, and M. V. Ramana. The frontiers of energy. *Nature Energy*, 1(1), January 2016.
- [6] Hongli Zhu, Wei Luo, Peter N. Ciesielski, Zhiqiang Fang, J. Y. Zhu, Gunnar Henriksson, Michael E. Himmel, and Liangbing Hu. Wood-derived materials for green electronics, biological devices, and energy applications. *Chemical Reviews*, 116(16):9305–9374, July 2016.
- [7] Karol Kulasinski, Sinan Keten, Sergey V. Churakov, Dominique Derome, and Jan Carmeliet. A comparative molecular dynamics study of crystalline, paracrystalline and amorphous states of cellulose. *Cellulose*, 21(3):1103–1116, March 2014.
- [8] Umesh P. Agarwal, Sally A. Ralph, Carlos Baez, Richard S. Reiner, and Steve P. Verrill. Effect of sample moisture content on XRD-estimated cellulose crystallinity index and crystallite size. *Cellulose*, 24(5):1971–1984, March 2017.
- [9] Patrik Ahvenainen, Inkeri Kontro, and Kirsi Svedström. Comparison of sample crystallinity determination methods by x-ray diffraction for challenging cellulose i materials. *Cellulose*, 23(2):1073–1086, February 2016.
- [10] L. Segal, J.J. Creely, A.E. Martin, and C.M. Conrad. An empirical method for estimating the degree of crystallinity of native cellulose using the x-ray diffractometer. *Textile Research Journal*, 29(10):786–794, October 1959.
- [11] Wayne A. Sisson. X-ray analysis of fibers. *Textile Research*, 3(6):295–307, April 1933.

- [12] Diana Ciolacu, Florin Ciolacu, and Valentin I Popa. Amorphous cellulose—structure and characterization. *Cellulose chemistry and technology*, 45(1):13, 2011.
- [13] NE Cusack. Amorphous metals. *IAEA, Wien*, 1987.
- [14] Mariel E Schmidt, William H Farrand, Jeffrey R Johnson, Christian Schröder, Joel A Hurowitz, Timothy J McCoy, Steven W Ruff, Raymond E Arvidson, David J Des Marais, Kevin W Lewis, et al. Spectral, mineralogical, and geochemical variations across home plate, gusev crater, mars indicate high and low-temperature alteration. *Earth and Planetary Science Letters*, 281(3-4):258–266, 2009.
- [15] Richard V Morris, David T Vaniman, David F Blake, Ralf Gellert, Steve J Chipera, Elizabeth B Rampe, Douglas W Ming, Shaunna M Morrison, Robert T Downs, Allan H Treiman, et al. Silicic volcanism on mars evidenced by tridymite in high-sio₂ sedimentary rock at gale crater. *Proceedings of the National Academy of Sciences*, 113(26):7071–7076, 2016.
- [16] Edgar U Zorn, Michael C Rowe, Shane J Cronin, Amy G Ryan, Lori A Kennedy, and James K Russell. Influence of porosity and groundmass crystallinity on dome rock strength: a case study from mt. taranaki, new zealand. *Bulletin of Volcanology*, 80:1–17, 2018.
- [17] Michael C Rowe, Ben S Ellis, and Abbie Lindeberg. Quantifying crystallization and devitrification of rhyolites by means of x-ray diffraction and electron microprobe analysis. *American Mineralogist*, 97(10):1685–1699, 2012.

- [18] RV Morris, CN Achilles, SJ Chipera, DW Ming, and EB Rampe. X-ray diffraction reference intensity ratios of amorphous and poorly crystalline phases: Implications for chemin on the mars science laboratory. In *Lunar and Planetary Science Conference*, 2013.
- [19] Patrik Ahvenainen, Inkeri Kontro, and Kirsi Svedström. Comparison of sample crystallinity determination methods by x-ray diffraction for challenging cellulose i materials. *Cellulose*, 23(2):1073–1086, 2016.
- [20] Sunghyun Nam, Alfred D. French, Brian D. Condon, and Monica Concha. Segal crystallinity index revisited by the simulation of x-ray diffraction patterns of cotton cellulose i and cellulose ii. *Carbohydrate Polymers*, 135:1–9, January 2016.
- [21] W. H. Bragg. The reflection of x-rays by crystals. *Nature*, 91(2280):477–477, 1913.
- [22] J. C. Kendrew, G. Bodo, H. M. Dintzis, R. G. Parrish, H. Wyckoff, and D. C. Phillips. A three-dimensional model of the myoglobin molecule obtained by x-ray analysis. *Nature*, 181(4610):662–666, 1958.
- [23] Takeshi Egami and Billinge S. J. L. *Underneath the Bragg Peaks Structural Analysis of Complex Materials*. Pergamon, 2012.
- [24] J. S. Wilkie. Carl nägeli and the fine structure of living matter. *Nature*, 190(4782):1145–1150, June 1961.
- [25] André Guinier. *X-ray diffraction: In crystals, imperfect crystals, and amorphous bodies*. Dover Publications, 2013.

- [26] P. Debye. Zerstreuung von röntgenstrahlen. *Annalen der Physik*, 351(6):809–823, 1915.
- [27] F. Zernike and J. A. Prins. Die beugung von röntgenstrahlen in flüssigkeiten als effekt der molekülaranordnung. *Zeitschrift für Physik A Hadrons and nuclei*, 41(2-3):184–194, 1927.
- [28] Xuelong Wang, Sha Tan, Xiao-Qing Yang, and Enyuan Hu. Pair distribution function analysis: Fundamentals and application to battery materials. *Chinese Physics B*, 29(2):028802, 2020.
- [29] Shahriar Karim Saurov, Aleksandra Mikhailidi, Kirsi Svedström, and Nina Kotelnikova. Comparative study of powder celluloses and cellulose hydrogels by waxes method.: Impact of measurement technique and computation on variability of results. *Cellulose chemistry and technology*, 53(9-10):885–896, 2019.
- [30] Anders Thygesen, Jette Oddershede, Hans Lilholt, Anne Belinda Thomsen, and Kenny Ståhl. On the determination of crystallinity and cellulose content in plant fibres. *Cellulose*, 12(6):563–576, August 2005.
- [31] Christopher J. Garvey, Ian H. Parker, and George P. Simon. On the interpretation of x-ray diffraction powder patterns in terms of the nanostructure of cellulose i fibres. *Macromolecular Chemistry and Physics*, 206(15):1568–1575, August 2005.
- [32] H. M. Rietveld. A profile refinement method for nuclear and magnetic structures. *Journal of Applied Crystallography*, 2(2):65–71, June 1969.

- [33] Laysa Pires De Figueiredo and Fabio Furlan Ferreira. The rietveld method as a tool to quantify the amorphous amount of microcrystalline cellulose. *Journal of Pharmaceutical Sciences*, 103(5):1394–1399, May 2014.
- [34] Rafael P. Oliveira and Carlos Driemeier. CRAFS: a model to analyze two-dimensional x-ray diffraction patterns of plant cellulose. *Journal of Applied Crystallography*, 46(4):1196–1210, July 2013.
- [35] W. Ruland. X-ray determination of crystallinity and diffuse disorder scattering. *Acta Crystallographica*, 14(11):1180–1185, November 1961.
- [36] Charles Kittel. *Introduction to Solid State Physics*. Wiley, 8 edition, 2004.
- [37] M. F. C. Ladd. The accurate interpolation of atomic scattering factors. *Zeitschrift für Kristallographie*, 123(5):373–381, November 1966.
- [38] L. R. M. Morin. Molecular form factors and photon coherent scattering cross sections of water. *Journal of Physical and Chemical Reference Data*, 11(4):1091–1098, October 1982.
- [39] Hongji Yuan and David L. Bish. NEWMOD, a new version of the NEWMOD program for interpreting x-ray powder diffraction patterns from interstratified clay minerals. *Clays and Clay Minerals*, 58(3):318–326, June 2010.
- [40] Monica Ferro, Alberto Mannu, Walter Panzeri, Con H.J. Theeuwen, and Andrea Mele. An integrated approach to optimizing cellulose mercerization. *Polymers*, 12(7):1559, July 2020.
- [41] Jie Gong, Jun Li, Jun Xu, Zhouyang Xiang, and Lihuan Mo. Research on cel-

lulose nanocrystals produced from cellulose sources with various polymorphs.

RSC Advances, 7(53):33486–33493, 2017.

Appendix

Crystalline Silicon Powder Datasheet, 100+200 MESH, 99.99% (METALS BASIS)



FICHA DE DATOS DE SEGURIDAD

Fecha de revisión 14-feb-2020

Número de Revisión 2

SECCIÓN 1: Identificación de la sustancia o la mezcla y de la sociedad o la empresa

Nombre Del Producto	Silicon powder, crystalline
Cat No. :	45609
Nº. CAS	7440-21-3
Sinónimos	No hay información disponible
Uso recomendado	Productos químicos de laboratorio.
Usos desaconsejados	Alimentos, drogas, pesticidas o productos biocidas.
<u>Datos del proveedor de la ficha de datos de seguridad</u>	

Company
Alfa Aesar
Thermo Fisher Scientific Chemicals, Inc.
30 Bond Street
Ward Hill, MA 01835-8099
Tel: 800-343-0660
Fax: 800-322-4757
Email: tech@alfa.com
www.alfa.com

Emergency Telephone Number
Durante el horario normal (de lunes a viernes de 8 am a 7 pm, hora), llame al (800) 343 a 0660.
Después de horas de oficina, llame Carechem 24 al (866) 928-0789.

SECCIÓN 2: Identificación de los peligros

Clasificación

Este producto químico se considera peligroso de acuerdo con la Norma de comunicación de peligros OSHA de 2012 (29 CFR 1910.1200)

Sólidos inflamables	Categoría 2
<u>Elementos de la etiqueta</u>	

Palabras de advertencia
Atención

Indicaciones de peligro
Sólido inflamable

**Consejos de prudencia****Prevención**

Mantener alejado de fuentes de calor, chispas, llama abierta o superficies calientes. - No fumar
 Conectar a tierra/enlace equipotencial del recipiente y del equipo de recepción
 Utilizar un material eléctrico/de ventilación/iluminación/ antideflagrante
 Llevar guantes/prendas/gafas/máscara de protección

Incendio

En caso de incendio: Utilizar CO₂, polvo seco o espuma como método de extinción

Peligros no clasificados de otra manera (HNOC)

Ninguno identificado

SECCIÓN 3: Composición/información sobre los componentes

Componente	Nº. CAS	Porcentaje en peso
Silicio	7440-21-3	>95

SECCIÓN 4: Primeros auxilios**Contacto con los ojos**

Enjuagar inmediatamente con abundante agua, también bajo los párpados, durante al menos 15 minutos. Consultar a un médico.

Contacto con la piel

Lavar inmediatamente con jabón y abundante agua y quitarse la ropa y el calzado contaminados. En caso de irritación de la piel o reacciones alérgicas, llamar a un médico.

Inhalación

Alejarse de la fuente de exposición, tumbarse en el suelo. Transportar a la víctima al exterior. Consultar a un médico.

Ingestión

Limpiar la boca con agua. Consultar a un médico.

Síntomas y efectos más importantes

No hay información disponible.

Notas para el médico

Tratar los síntomas

SECCIÓN 5: Medidas de lucha contra incendios**Medios de extinción apropiados**

Producto químico seco. Polvo(s). Arena seca.

Medios de extinción no apropiados

Agua

Punto de Inflamación

No hay información disponible

Método -

No hay información disponible

Temperatura de autoignición

150 °C / 302 °F

Límites de explosión**Superior**

No hay datos disponibles

Inferior

No hay datos disponibles

Sensibilidad a impactos mecánicos

No hay información disponible

Sensibilidad a descargas estáticas No hay información disponible

Peligros específicos que presenta el producto químico

Inflamable. Puede entrar en ignición por efecto de calor, chispas o llamas.

Productos de combustión peligrosos

Dióxido de silicio.

Equipo de protección y medidas de precaución para el personal de lucha contra incendios

Como en cualquier incendio, llevar un aparato de respiración autónomo de presión a demanda MSHA/NIOSH (aprobado o equivalente) y todo el equipo de protección necesario.

NFPA

Salud	Inflamabilidad	Inestabilidad	Peligros físicos
1	3	0	N/A

SECCIÓN 6: Medidas en caso de vertido accidental

Precauciones personales	Utilizar el equipo de protección individual obligatorio. Evitar la formación de polvo. Retirar todas las fuentes de ignición. Evítense la acumulación de cargas electroestáticas.
Precauciones relativas al medio ambiente	No debe liberarse en el medio ambiente. Para obtener más información ecológica, ver el apartado 12.
Métodos de contención y limpieza	Barrer y recoger en contenedores apropiados para su eliminación. Evitar la formación de polvo. Retirar todas las fuentes de ignición. Utilizar herramientas que no hagan chispas y un equipamiento a prueba de explosiones.

SECCIÓN 7: Manipulación y almacenamiento

Manipulación	Evítese el contacto con los ojos y la piel. No respirar el polvo. Evítense la acumulación de cargas electroestáticas. Manipular el producto únicamente en sistemas cerrados o proporcionar una ventilación por extracción adecuada. Utilizar únicamente herramientas que no produzcan chispas. Utilizar herramientas que no hagan chispas y un equipamiento a prueba de explosiones. Tomar las medidas necesarias para evitar descargas de electricidad estática (que podrían provocar la ignición de vapores orgánicos).
Almacenamiento	Mantener en un lugar fresco, seco y bien ventilado. Mantener el recipiente herméticamente cerrado. Área de productos inflamables. Mantener alejado de fuentes de calor, chispas, llama abierta o superficies calientes. - No fumar.

SECCIÓN 8: Controles de exposición / protección personal

Pautas relativas a la exposición

Componente	ACGIH TLV	OSHA PEL	NIOSH IDLH	Mexico OEL (TWA)
Silicio		(Vacated) TWA: 10 mg/m ³ (Vacated) TWA: 5 mg/m ³ TWA: 15 mg/m ³ TWA: 5 mg/m ³	TWA: 10 mg/m ³ TWA: 5 mg/m ³	

Leyenda

OSHA Administración de Seguridad y Salud

NIOSH IDLH: NIOSH - Instituto Nacional para la Salud y Seguridad Ocupacional, National Institute for Occupational Safety and Health

Medidas técnicas Asegurar una ventilación adecuada, especialmente en áreas confinadas.

Equipo de protección personal

Protección ocular y de la cara: Utilizar lentes de protección adecuados o gafas para productos químicos como se describe

en las normas para la protección de los ojos y la cara de la OSHA, en 29 CFR 1910.133.

Protección de la piel y el cuerpo Utilizar guantes y ropa de protección adecuados para evitar la exposición de la piel.

Protección respiratoria No necesario usar equipo protector en las condiciones normales de su uso.

Medidas higiénicas Manipular respetando las buenas prácticas de higiene industrial y seguridad.

SECCIÓN 9: Propiedades físicas y químicas

Estado físico	Polvo(s) Sólido
Aspecto	Gris oscuro
Olor	Inodoro
Umbral olfativo	No hay información disponible
pH	No hay información disponible
Punto/intervalo de fusión	1410 °C / 2570 °F
Punto /intervalo de ebullición	2355 °C / 4271 °F @ 760 mmHg
Punto de Inflamación	No hay información disponible
Índice de Evaporación	No es aplicable
Inflamabilidad (sólido, gas)	No hay información disponible
Inflamabilidad o explosión	
Superior	No hay datos disponibles
Inferior	No hay datos disponibles
Presión de vapor	No hay información disponible
Densidad de vapor	No es aplicable
Densidad relativa	No hay información disponible
Solubilidad	No hay información disponible
Coeficiente de reparto octanol: agua	No hay datos disponibles
Temperatura de autoignición	150 °C / 302 °F
Temperatura de descomposición	No hay información disponible
Viscosidad	No es aplicable
Fórmula molecular	Si
Peso molecular	28.09

SECCIÓN 10: Estabilidad y reactividad

Riesgo de reacción	Ninguno conocido, en base a la información facilitada.
Estabilidad	Estable en condiciones normales.
Condiciones que deben evitarse	Exceso de calor. Productos incompatibles. Mantener alejado de llamas desnudas, superficies calientes y fuentes de ignición.
Materiales incompatibles	Agentes oxidantes fuertes, Ácidos
Productos de descomposición peligrosos	Dióxido de silicio
Polimerización peligrosa	No se produce ninguna polimerización peligrosa.
Reacciones peligrosas	Ninguno durante un proceso normal.

SECCIÓN 11: Información toxicológica

Toxicidad aguda

Información del producto

Información sobre los componentes

Componente	DL50 Oral	DL50 cutánea	LC50 Inhalación
Silicio	LD50 = 3160 mg/kg (Rat)	No figura en la lista	No figura en la lista

Productos Toxicológicamente Sinergísticos	No hay información disponible					
Efectos retardados e inmediatos, así como efectos crónicos producidos por una exposición a corto y largo plazo						
Irritación	No hay información disponible					
Sensibilización	No hay información disponible					
Carcinogenicidad	La tabla siguiente indica si cada agencia ha incluido alguno de los componentes en su lista de carcinógenos.					
Componente	Nº CAS	IARC	NTP	ACGIH	OSHA	México
Silicio	7440-21-3	No figura en la lista				
Efectos mutagénicos	No hay información disponible					
Efectos sobre la reproducción	No hay información disponible.					
Efectos sobre el desarrollo	No hay información disponible.					
Teratogenicidad	No hay información disponible.					
STOT - exposición única	Ninguno conocido					
STOT - exposición repetida	Ninguno conocido					
Peligro por aspiración	No hay información disponible					
Síntomas / efectos, agudos y retardados	No hay información disponible					
Información del alterador del sistema endocrino	No hay información disponible					
Otros efectos adversos	No se han estudiado completamente las propiedades toxicológicas.					

SECCIÓN 12: Información Ecológica

Ecotoxicidad

No tirar los residuos por el desague.

Persistencia/ Degradabilidad	Insoluble en agua
Bioacumulación	No hay información disponible.
Movilidad	No es probable que sea móvil en el medio ambiente debido a su baja solubilidad en agua.

SECCIÓN 13: Consideraciones relativas a la eliminación

Métodos de eliminación de los desechos	Quienes generen residuos químicos deberán determinar si los productos químicos desechados se clasifican como residuos peligrosos. Los generadores de residuos químicos deberán consultar también las normativas locales, regionales y nacionales relativas a residuos peligrosos con el fin de asegurar una clasificación completa y exacta.
---	--

SECCIÓN 14: Información relativa al transporte

DOT

Nº ONU	1346
Designación oficial de transporte	SILICIO EN POLVO, AMORFO
Clase de peligro	4.1
Grupo de embalaje	III
TDG	
Nº ONU	1346

Designación oficial de transporte	SILICIO EN POLVO, AMORFO
Clase de peligro	4.1
Grupo de embalaje	III
IATA	
Nº ONU	UN1346
Designación oficial de transporte	SILICIO EN POLVO, AMORFO
Clase de peligro	4.1
Grupo de embalaje	III
IMDG/IMO	
Nº ONU	UN1346
Designación oficial de transporte	SILICIO EN POLVO, AMORFO
Clase de peligro	4.1
Grupo de embalaje	III

SECCIÓN 15: Información reglamentaria

United States of America Inventory

Componente	Nº. CAS	TSCA	TSCA Inventory notification - Active/Inactive	TSCA - EPA Regulatory Flags
Silicio	7440-21-3	X	ACTIVE	-

Leyenda:

TSCA - Toxic Substances Control Act, (40 CFR Part 710)

X - Incluido

'-' - No listado

TSCA 12 (b) - Avisos de exportación No es aplicable

Inventarios internacionales

Canadá (DSL/NDSL), Europa (EINECS/ELINCS/NLP), Filipinas (PICCS), Japan (ENCS), Australia (AICS), China (IECSC), Korea (ECL).

Componente	Nº. CAS	DSL	NDSL	EINECS	PICCS	ENCS	AICS	IECSC	KECL
Silicio	7440-21-3	X	-	231-130-8	X	X	X	X	KE-31029

Reglamentaciones Federales

SARA 313 No es aplicable

Categorías de riesgos SARA 311/312 Para más información, ver la sección 2

CWA (Ley del agua limpia, Clean Water Act) No es aplicable

Ley del Aire Limpio No es aplicable

OSHA - Administración de Seguridad y Salud No es aplicable

CERCLA No es aplicable

Proposición 65 de California Este producto no contiene ninguna sustancia química de la Proposición 65.

Normativas estatales de derecho a la información de los EE.UU

Componente	Massachusetts	Nueva Jersey	Pennsylvania	Illinois	Rhode Island
------------	---------------	--------------	--------------	----------	--------------

Silicio	X	X	X	-	X
---------	---	---	---	---	---

Departamento de Transporte de EE.UU.

Cantidad Reportable (RQ): N
Contaminante marino DOT N
DOT Severe Marine Pollutant N

Departamento de Seguridad Nacional de EE.UU. Este producto no contiene ningún ingrediente de DHS.

Otras regulaciones internacionales

México - Grado No hay información disponible

SECCIÓN 16: Otra información

Preparado por Departamento de seguridad del producto
Email: tech@alfa.com
www.alfa.com

Fecha de revisión 14-feb-2020
Fecha de impresión 14-feb-2020
Resumen de la revisión SDS authoring systems update, replaces ChemGes SDS No. 7440-21-3/1.

Descargo de responsabilidad

La información facilitada en esta Ficha de Datos de Seguridad es correcta, a nuestro leal saber y entender, en la fecha de su publicación. Dicha información está concebida únicamente como guía para la seguridad en la manipulación, el uso, el procesamiento, el almacenamiento, el transporte, la eliminación y la liberación, no debiendo tomarse como garantía o especificación de calidades. La información se refiere únicamente al material específico mencionado y puede no ser válida para tal material usado en combinación con cualesquiera otros materiales o en cualquier proceso salvo que se especifique expresamente en el texto

Fin de la FDS

Variable Counting Time Experiment

Experiment overview

0	1	2
Application type	PowderDiffraction (Standard)	
Experiment time	20574 [s]	
Expansion model	Standard	
Identifier		
	Creation time	Friday, March 24, 2023:11:29:00 AM
	Machine	DESKTOP-USIIBK2
	GUID	ef71771b-37c2-4021-8328-758f42e69a34

Measurement setup overview

0	1
User	Lab Manager
Comment	Time/step variable para angulos grandes
Sequences	(none)
XY positions	(none)
Profiles	(none)

Methods

0	1	2	3	4	5	6
Method #1						
	Scan setup	Coupled TwoTheta/Theta				
		ScanMode	Continuous PSD fast			
		Scan axes				
		2Theta				
			AbsoluteStart 5.0001 [°]			
			AbsoluteStop 120.0039815761 [°]			
		Theta				
			AbsoluteStart 2.50005 [°]			
			AbsoluteStop 60.00199078805 [°]			
		PSD opening				
			AbsoluteFixed 2.9493426432 [°]			
	Method expander (s)					
		Manual				
		Sub-scan list	from [°]	to [°]	steps	time/step [s]
		1	5.0001	30.0001	1221	1
		2	30.0001	60.0001	2929	1.5
		3	60.0001	92.0001	3125	2
		4	92.0001	120.0039	2735	2.5
	Used detector(s)					
		LYNXEYE_XE (1D mode)				
			LowerDiscriminator	0.21 [V]		
			UpperDiscriminator	0.234 [V]		
			Veto	0.04 [V]		
	Fixed drives					
	Sample rotation					
		Phi				
			RotationSpeed	21 [/min]		
	Instrument					
		Primary track(s)				
		PrimaryTrack	radius	280 [mm]		
			TubeMount	Bank position	1	
			Tube	Tube		
				WaveLengthAlpha1	1.5406 [Å]	
				WaveLengthAlpha2	1.54439 [Å]	
				WaveLengthAverage	1.5418 [Å]	
				WaveLengthBeta	1.39222 [Å]	

				WaveLengthRatio	0.5 []	
				FocusOrientation	1 []	
				FocusOrientation Text	Line Focus	
				WindowThickness	-1 [mm]	
				SerialNumber	0 []	
				TypeNumber	1 []	
				TubeMaterial	Cu	
				Generator	Generator	
				Voltage	50 [kV]	
				Current	20 [mA]	
		Twin_Primary	Bank position	2		
		No Slit 10.5 [mm]	Bank position	3		
			Height	10.5 [mm]		
			SlitID	No Slit		
			SlitIDValue	0 []		
	Secondary track (s)					
	SecondaryTrack	radius	280 [mm]			
		LYNXEYE_XE	Bank position	18		
		No Slit 10.5 [mm]	Bank position	11		
			Height	10.5 [mm]		
			SlitID	No Slit		
			SlitIDValue	0 []		
		Twin_Secondary	Bank position	10		
	Goniometer center					
	Stage	Rotation Stage				

Sequences, XY positions and profiles

0	1
Sequences	(none)

XY positions

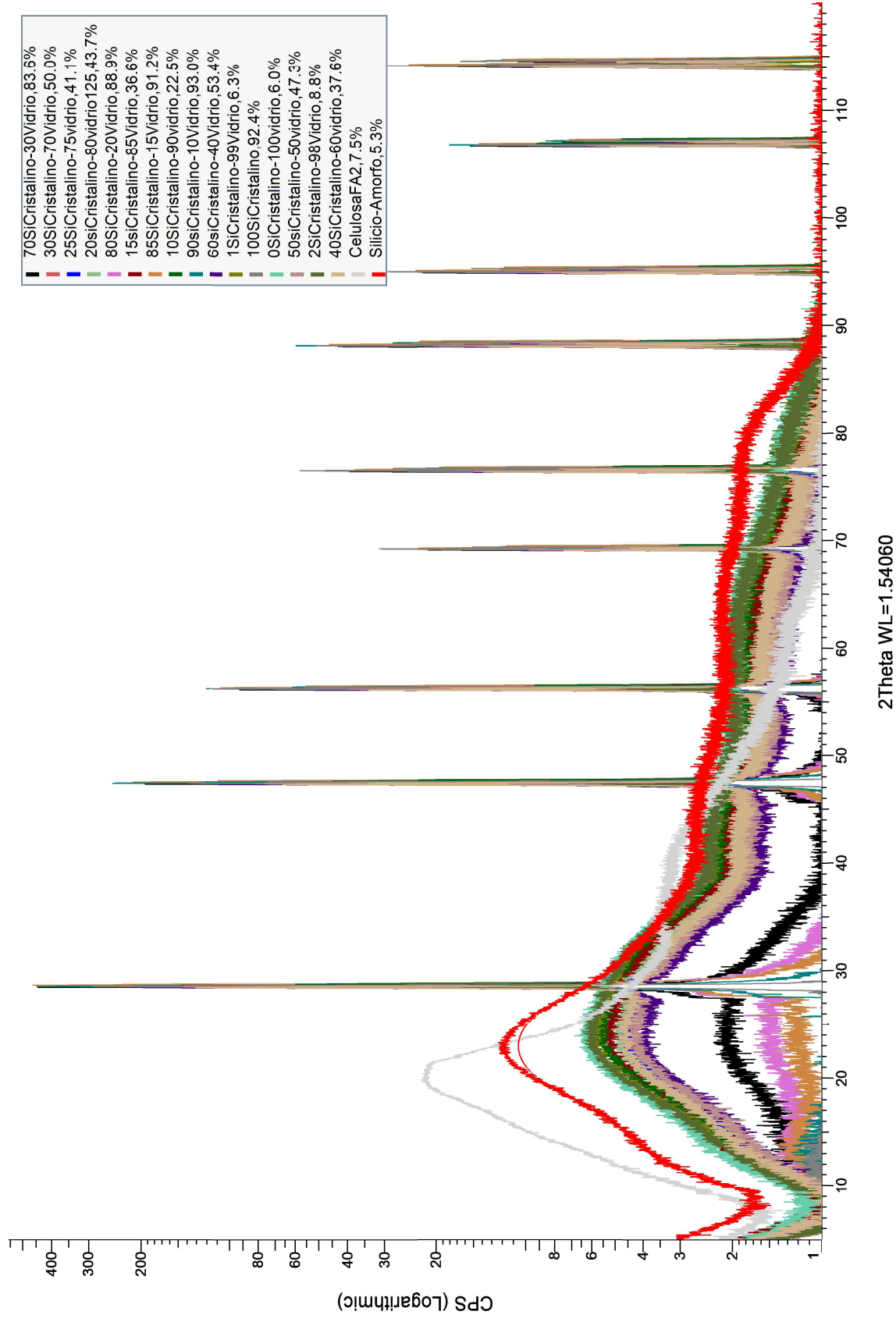
	0
	(none)

Profiles

0	1
Profiles	(none)

Crystallinity Index by DIFFRAC.EVA (by Bruker)

70SiCristalino-30Vidrio (Coupled TwoTheta/Theta)



100SiCristalino (Coupled TwoTheta/Theta)

